minerals

MDPI

Article

A Data-Driven Approach to the Unified Evaluation of Conventional and Unconventional Hydrocarbon Resources: Application to Low-Mature to Mature Source Rocks in the Liaohe Western Depression

Shasha Hui [1,2], Xiongqi Pang [1,2,*], Hong Pang [1,2,*], Changrong Li [3], Xiaolong Zhou [4], Tao Hu [1,2], Kanyuan Shi [1,2], Min Li [1,2], Shuxing Mei [1,2], Wu Yuan [5] and Jianping Cheng [4]

[1] State Key Laboratory of Petroleum Resources and Prospecting, China University of Petroleum (Beijing), Beijing 102249, China
[2] College of Geosciences, China University of Petroleum (Beijing), Beijing 102249, China
[3] School of Earth and Space Sciences, Peking University, Beijing 100871, China
[4] Exploration and Development Research Institute, PetroChina Liaohe Oilfield Company, Panjin 124010, China
[5] Shenyang Oil Production Plant, PetroChina Liaohe Oilfield Company, Shenyang 110316, China
* Correspondence: pangxq@cup.edu.cn (X.P.); panghong19820107@126.com (H.P.)

Abstract: Hydrocarbon potential evaluation is a high priority in oil/gas exploration which is significantly influenced by evaluation methods and subjective cognition. With the aim of quantitatively establishing a hydrocarbon generation and expulsion (HGE) model of source rocks, a data-driven approach is proposed based on abundant and readily available Rock-Eval/total organic carbon content (TOC)/vitrinite reflectance (VRo) datasets. This approach takes into account the original hydrocarbon generation potential (GPIo) and the loss of TOC. Hydrocarbon generation simulation was also adopted in this study. This data-driven method was applied to the Lower Paleogene Shahejie Formation (Es4), which has three sets of superior source rocks (average thickness > 250 m, TOC > 3%). The GPIo of the Es4 low-maturity source rock was 600 mg HC/g TOC. The initial maturity values of hydrocarbon generation and expulsion were 0.36% and 0.46%, respectively. The Gaosheng sub-member of the Es4 source rock had the largest amount of hydrocarbon generation but a limited amount of hydrocarbon expulsion, implying a favorable exploration of shale oil resources. By contrast, the values of the conventional, unconventional tight, and shale oil resource potentials of the Niuxintuo sub-member were 3.20×10^7, 7.70×10^7, and 5.93×10^8 t, respectively, indicating good prospects for tight oil and shale oil exploration. A comparison between the previous method and the data-driven method showed considerable differences in the restoration of GPIo and TOC, and both had their own limitations. This data-driven approach provides a quick and valid source rock evaluation method and can greatly enhance the accuracy of resource assessment.

Keywords: geochemical characteristics; hydrocarbon generation potential method; numerical analysis; resource evaluation; low-maturity source rock

Citation: Hui, S.; Pang, X.; Pang, H.; Li, C.; Zhou, X.; Hu, T.; Shi, K.; Li, M.; Mei, S.; Yuan, W.; et al. A Data-Driven Approach to the Unified Evaluation of Conventional and Unconventional Hydrocarbon Resources: Application to Low-Mature to Mature Source Rocks in the Liaohe Western Depression. *Minerals* **2023**, *13*, 390. https://doi.org/10.3390/min13030390

Academic Editor: Thomas Gentzis

Received: 7 February 2023
Revised: 6 March 2023
Accepted: 8 March 2023
Published: 10 March 2023

1. Introduction

With the improvement of existing exploration technology and rapid growth in energy demands, China has gradually shifted from conventional and shallow oil/gas exploration to unconventional and deep oil/gas exploration, especially in the petroliferous basins of eastern China [1]. Moreover, in recent decades, an increasing number of studies on unconventional shale oil and gas resource evaluation and CO_2 sequestration, aiming to enhance oil recovery, have been carried out outside China so as to supplement the shortage of conventional oil and gas resources [2–4]. Therefore, an objective method for evaluating both conventional and unconventional hydrocarbon resource potentials is indispensable.

In recent decades, previous evaluation methods of conventional and unconventional hydrocarbon resource potentials have made significant contributions, such as genetic, analogy, statistical, small-surface-element volume, and estimated ultimate recovery (EUR) analogy methods, as well as resource spatial distribution mapping [5–9]. However, given the diversity and subjectivity of these methods, the evaluation of hydrocarbon resource potential in the same basin can vary considerably and can be viewed as unreliable. In addition, none of the abovementioned methods takes into account low-maturity source rocks, even though low-mature oil is widely distributed and non-negligible. Organic-rich rocks are a source of hydrocarbons produced from conventional reservoirs and can also serve as a reservoir for unconventional resources [10,11]. Pang et al. [12] proposed a material-balanced model for hydrocarbon generation, expulsion, and retention during the thermal evolution of source rocks. The model has the advantage of simulating the dynamic variation in the hydrocarbon generation potential of source rocks from the immature to high-mature stages and overcomes the heterogeneity of source rocks by incorporating data from multiple samples. To date, this method has been verified and incrementally improved by later researchers [13–17]. Considering the aspect of inert carbon conservation, this method was revised to restore the original TOC so as to determine the original hydrocarbon generation potential index (GPIo) [11,13,16]. Additionally, instead of burial depth, vitrinite reflectance (VRo) was chosen as the parameter to reduce the effect of tectonic activity [13,14]. Furthermore, hydrocarbon evaporative loss during the process of collecting samples was considered [15,18].

It is noteworthy that some shortcomings still exist. The determination of GPIo in previous studies was mainly based on the hand-drawn envelope curve of the Rock-Eval/TOC dataset, which is vulnerable to problems with data distribution and human subjectivity. Additionally, the restoration coefficient k proposed by later researchers to recover the TOC loss increases exponentially with increasing thermal maturity, leading to an overestimation of hydrocarbon resource potential [13]. Finally, and most importantly, the hydrocarbon generation threshold (HGT) defaulted as VRo = 0.5% was considered to be imprecise [19], since it does not take into account differences in organic matter (OM) types, hampering the resource evaluation of low-maturity source rocks. In view of the problems mentioned above, an optimized method that can be used to accurately evaluate hydrocarbon resource potentials is significant. Great progress has been made in the conventional resource exploration of the Liaohe Western Depression, Bohai Bay Basin (Figure 1) [20]. However, due to the lack of systematic evaluation of the source rocks, the great resource potential in the study area has been overlooked. The inaccuracy of resource evaluation results and technology restrictions limit the exploration of unconventional resources.

As described in this paper, a data-driven model was quantitatively established to characterize hydrocarbon generation and expulsion (HGE) characteristics. This data-driven approach was realized by the numerical analysis of abundant and readily available Rock-Eval/TOC/VRo datasets and can reduce the influences of the heterogeneity of source rocks and human subjectivity. Considering the limited thermal maturity range of source rocks in the study area, hydrocarbon generation simulation was also adopted to supplement the datasets, which greatly improved the reliability of the model. This study aimed to: (1) precisely restore the GPIo and original TOC (TOCo) of source rocks; (2) determine the hydrocarbon generation threshold (HGT) and hydrocarbon expulsion threshold (HET) of low-maturity source rocks; and (3) evaluate the conventional and unconventional hydrocarbon resource potentials. This study is of great theoretical and practical significance for efforts to overcome the disadvantages of previous source rock evaluation methods and improve the evaluation accuracy of hydrocarbon resources, which can enhance the exploration benefits.

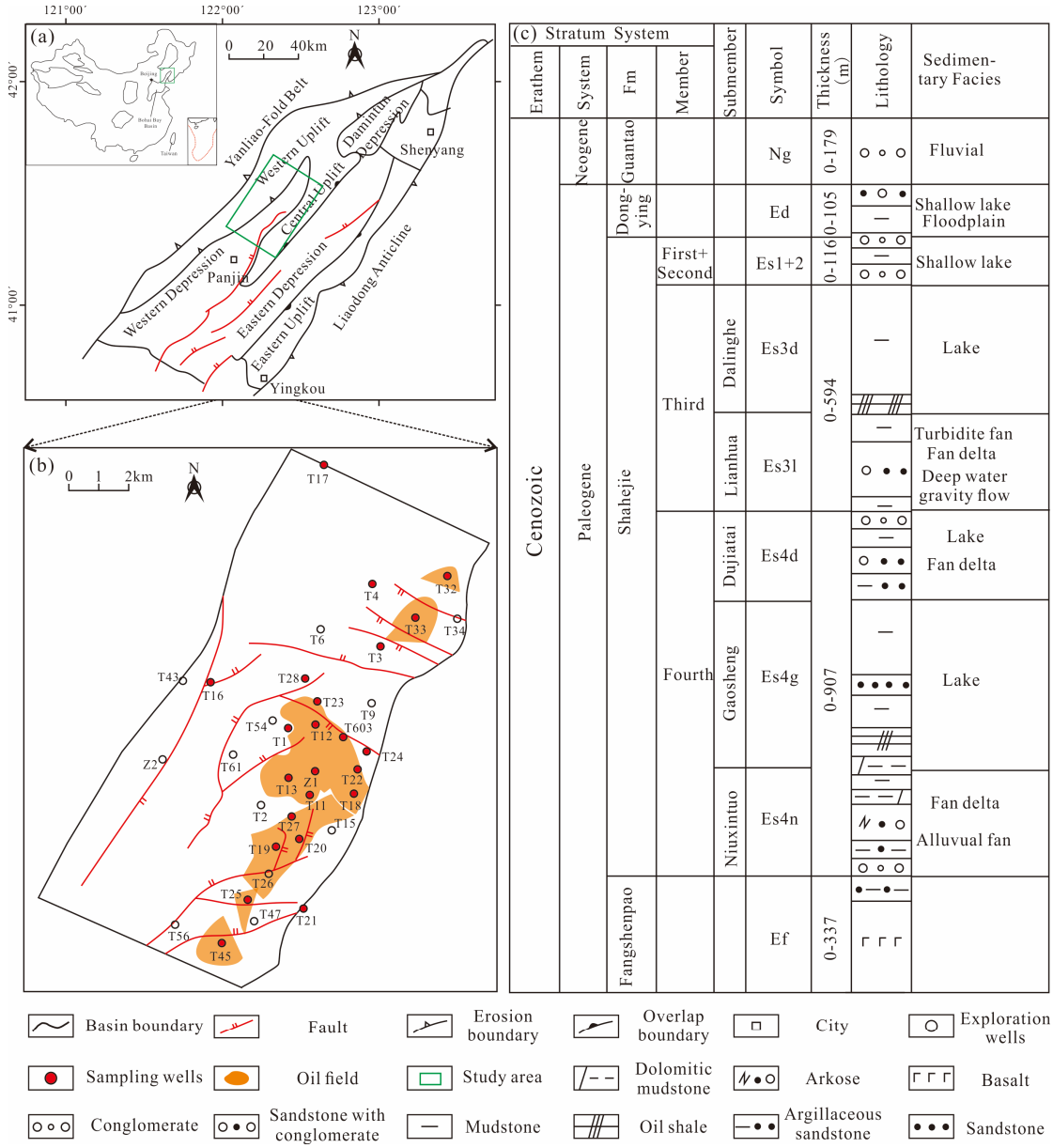

Figure 1. Map of the structural and stratigraphic characteristics of the Niuxintuo area, Liaohe Western Depression. (**a**) Tectonic units of Liaohe Depression. (**b**) Structural map of the Niuxintuo area. (**c**) Stratigraphic column map.

2. Geological Setting

2.1. Tectonic Setting

The Bohai Bay Basin is a Cenozoic rifted basin located on the eastern coast of China (Figure 1a) [21]. The study area, covering ~400 km^2, comprises the northernmost part of the Liaohe Western Depression in the northeast Bohai Bay Basin (Figure 1a,b). The strata are illustrated in Figure 1c. The study area has experienced four tectonic stages from the Paleogene to Quaternary [20,22,23]. The first stage was the initial extensional rift period during the Paleocene, with the deposition of the Fangshenpao Formation (Ef) (65–45.4 Ma). The Niuxintuo area was subjected to tensile forces, forming boundary faults oriented in the NNE direction. These faults (e.g., the Taian Fault) controlled the formation and evolution of the basin. The second stage was an intense rift period during the Eocene, with the deposition of the Es4 and Es3 members (45.4–38 Ma). The strata are extensive and thick [24]. The third stage was the strike-slip rift period during the Oligocene (38–24.6 Ma), which

resulted in the Dongying Formation (Ed). During the Oligocene, the regional stress field changed from rifting to strike-slip, creating a series of near-EW-oriented faults. The strata were uplifted and eroded (the maximum erosion thickness reached 1500 m), resulting in the general erosion of the upper Es3, Es2, and Es1 members and the Ed Formation. The fourth stage was the depression period from the Neogene to the Quaternary (24.6–0 Ma), in which the Guantao (Ng), Minghuazhen (Nm), and Quaternary Formations were formed, without any prominent faulting (Figure 2) [25].

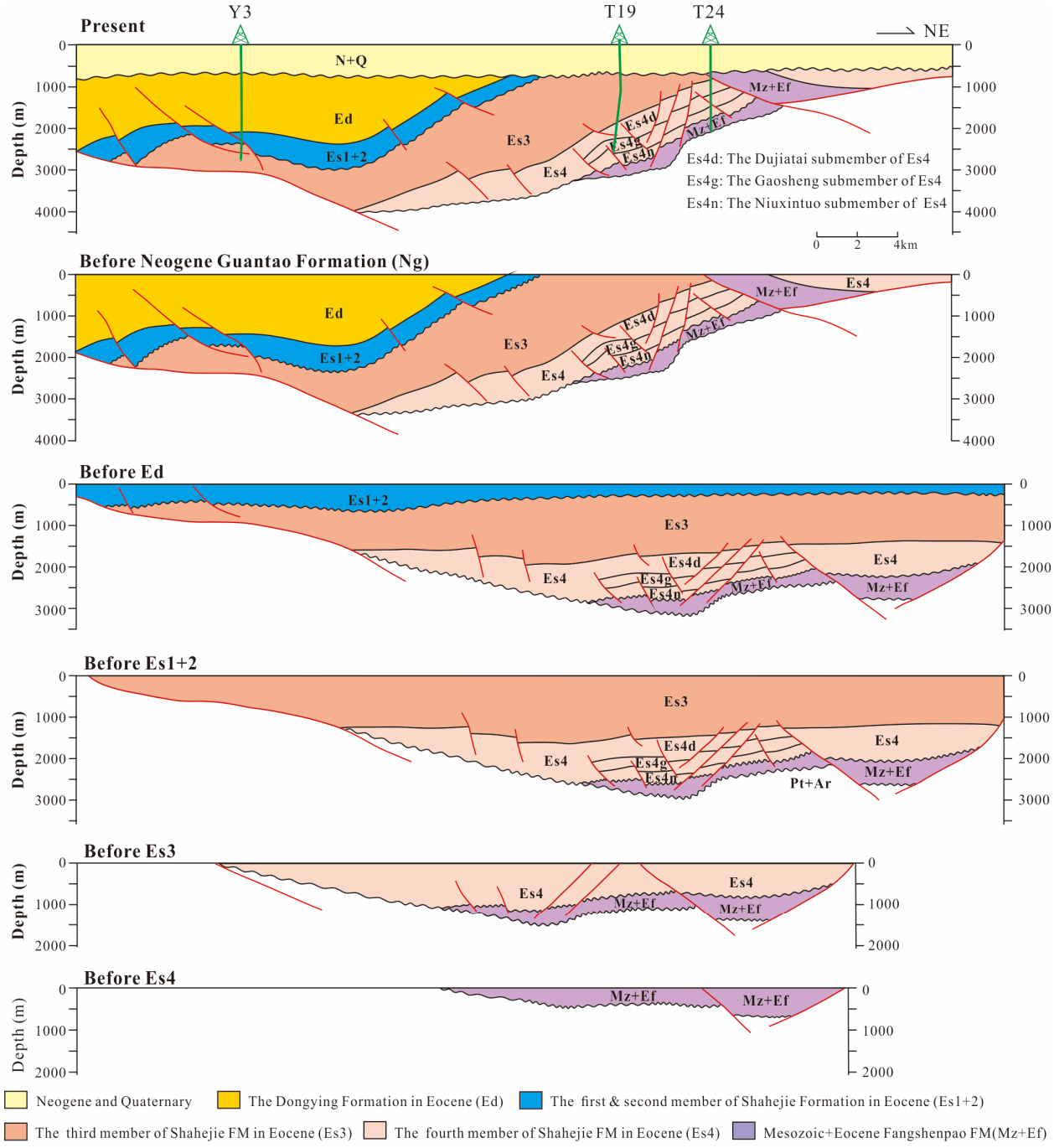

Figure 2. Profile of the tectonic evolution of the Niuxintuo area.

2.2. Sedimentary Environment

The sedimentary environment during the Paleogene mainly comprised thick nonmarine clastic deposits, with a small number of volcanic and carbonate rocks [25]. The Es4

member developed alluvial fan, fan delta, and semi-deep–deep lacustrine environments (Figure 1c), dominated by conglomerates, sandstones, mudstones, and shales, including the predominant source rocks and reservoir, regarded as self-generation and self-accumulation [24,26]. The Es4 member can be subdivided into the Niuxintuo sub-member (Es4n), Gaosheng sub-member (Es4g), and Dujiatai sub-member (Es4d) from the bottom to the top. The Es4n sub-member mainly developed a fan delta and shallow lacustrine environment, comprising conglomerates, mudstones, and local carbonate rocks (Figure 1c), indicating a moderately shallow-water saline environment. With the deepening of the water body and decrease in salinity, the carbonate content decreased, resulting in thick lacustrine mudstone in the Es4g and Es4n sub-members [27]. The Es4 member marked the beginning of a transgressive cycle that continued to the Es3 member [24]. The whole Es3 member was dominated by a deep freshwater lacustrine environment [21]. Because of violent subsidence activity, water inflow occurred, forming a broad semi-deep–deep lake and causing the deposition of thick dark mudstone in the Es3 member (Figure 1c) [25].

3. Material and Methods

3.1. Samples and Laboratory Instruments

In the Niuxintuo area, 129 source rock samples from 22 wells were used to analyze the geochemical characteristics. The 22 wells were located as evenly as possible across the study area, and all were drilled into the target formation, as shown in Figure 1c. The core samples were systematically collected from different depths to ensure that the samples were representative. The analytical experiments performed in this research included Rock-Eval pyrolysis (79 samples), TOC analysis (101 determinations), VRo measurements (54 samples), maceral analysis, group component analysis of crude oil (17 oil samples), and saturated hydrocarbon GC–MS analysis (18 samples). Furthermore, five low-mature shale samples deposited in a similar paleo-environment with different kerogen types in the Liaohe Western Depression were selected as the control group to conduct the hydrocarbon generation simulation experiment. Additional geochemical data of the Paleogene Shahejie source rocks of the Liaohe Western Depression were obtained from the PetroChina Liaohe Oilfield Company, Panjin, China.

The TOC contents were measured using a LECO CSe400 analyzer (St. Joseph, MI, USA). The Rock-Eval pyrolysis experiment was performed using the Rock-Eval VI instrument (Rock Eval 6, VINCI TECHNOLOGIES, Nanterre, France). When the S_2 was <0.2 mg/g, it was difficult to identify T_{max}, resulting in unreliable T_{max} data. Therefore, the screening standard 420 °C < T_{max} < 500 °C was introduced to establish the HGE model [28,29]. The mean random VRo was tested via oil immersion of the sample and its analysis at a wavelength of 546 nm using a Leica DM4500P polarizing microscope (Leica, Wetzlar, Germany) and a reflected-light 50× objective lens equipped with an TIDAS S MSP-200 photometer (J&M, Essingen, Germany) [30]. The determination of maceral components was performed using a fluorescence maceral identification method (SY/T 6414-1999) [31]. The group component analysis was performed on a silica gel–alumina column using different polar solvents. The Agilent 7980-5975c instrument (Agilent Scientific Instruments, Santa Clara, CA, USA) was used for the GC–MS analysis. During a GC–MS experiment, the temperature should initially be kept at 50 °C for 1 min and then be heated to 250 °C at 4 °C/min, continuing to 310 °C at 3 °C/min and being kept as constant for 30 min.

The hydrocarbon generation simulation was performed using a high-temperature–high-pressure thermal simulation instrument (OGE-II) at Lanzhou Institute of Geology, Chinese Academy of Sciences, Lanzhou, China. The prepared cylindrical samples were first sealed in the instrument, and each sample weighed approximately 60 to 80 g. After heating the thermostatic device, the temperature reached the specified temperature at a heating rate of 1 °C/min, which was maintained for 48 h. The experimental temperatures were designed to be 200, 250, 300, 350, 400, 450, and 500 °C, respectively. Moreover, the computer temperature automatic control system maintained the temperature accuracy at 0.2 °C. In order to simulate the real geological conditions, the strata and lithostatic pressures were

considered in this experiment. The experimental pressures were designed to be 50, 55, 60, 65, 70, 75, and 80 MPa, respectively. After the experiment, the hydrocarbon products and residual samples were collected. The produced gas was collected and measured immediately. After repeatedly flushing the instrument pipe, sample collector, and chamber with dichloromethane (DCM) solvent, a mixture of liquid hydrocarbons and DCM solvent was obtained. Then, the DCM solvent was removed from the mixed liquid, and the expelled oil was collected. The retention oil was obtained from residual samples by extraction of the DCM solvent. TOC analysis, Rock-Eval pyrolysis, Ro measurements, and Soxhlet extraction were performed on the simulated residual samples.

3.2. Methods

The hydrocarbon generation potential method was proposed, using a large number of Rock-Eval/TOC datasets to investigate the variation in the hydrocarbon generation potential with the VRo values so as to simulate the thermal evolution of source rocks (Figure 3a) [11]. According to the mass balance principle, the hydrocarbon potential of source rocks mainly includes three parts: (1) the kerogen or residual organic matter (OM) that has not been transformed into hydrocarbons (pyrolysis hydrocarbons: S_2); (2) the hydrocarbons that have been generated but not discharged (free hydrocarbons: S_1); and (3) the discharged hydrocarbons (Q_e) [11,32]. Considering that S_1 and S_2 are the actual quantitative measurements of the hydrocarbon generation capacity obtained through Rock-Eval pyrolysis [33], the hydrocarbon generation potential index (*GPI*) can be defined as $(S_1 + S_2)/TOC \times 100$, which reflects the current amount of hydrocarbons generated per unit of TOC by source rocks. Then, the variation in *GPI* with thermal maturity can be used to quantitatively characterize the hydrocarbon generation and expulsion of source rocks. The original *GPI* (*GPIo*) should remain unchanged before hydrocarbon expulsion ($Q_e = 0$). With increasing thermal maturity, the *GPI* of the source rock decreases, indicating that the hydrocarbons have been expelled.

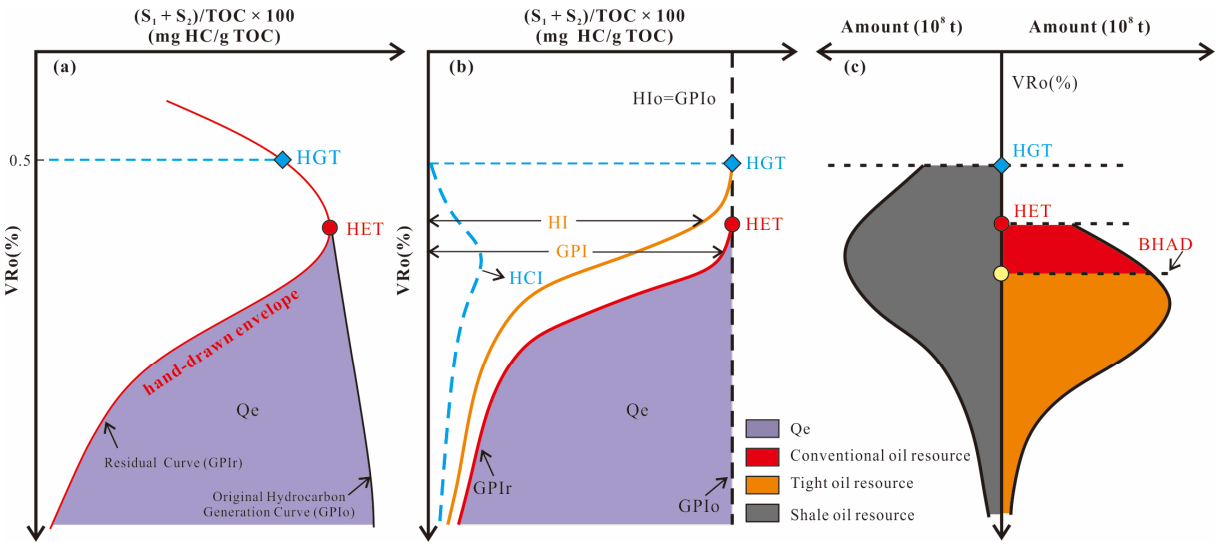

Figure 3. (**a**) Conceptual HGE model established by the traditional method proposed by Pang et al. [12]. (**b**) The optimized HGE model established by the data-driven approach. (**c**) The unified evaluation model for different hydrocarbon resources.

Rock-Eval/TOC datasets have been used extensively for studying kerogen hydrocarbon kinetics [16,34,35]. A statistical method was proposed for studying kerogen hydrocarbon kinetics according to variations in the hydrogen index (*HI*) as a function of T_{max} [33]:

$$HI = HIo \times \left(1 - \exp\left(-\left(\frac{Tmax}{\beta_1}\right)^{\theta_1}\right)\right) + c_1 \quad (1)$$

where $HI = (S_2/TOC) \times 100$ (mg HC/g TOC); β_1 and θ_1 are the parameters corresponding to the hydrocarbon generation kinetics, which depend on the shape of the fitting curve; and c_1 is a constant. When the source rock is immature or low-mature, $c = 0$. Notably, the resulting optimal *HIo* is the highest among the average values based on statistical analysis.

Numerical analysis can be used to quantitatively characterize the variations in *GPI* and *VRo* based on the abundant Rock-Eval/TOC datasets, as shown in Equation (2) [16]. For immature source rocks, *GPIo* is equal to *HIo*:

$$GPI = GPIo \times \left(1 - \exp(-(\frac{VRo}{\beta_2})^{\theta_2})\right) + c_2 \quad (2)$$

Based on the abovementioned regression relationship, the optimal *HIo* and *GPIo* are derived to determine the original hydrocarbon generation potential (Figure 3b). In addition, the transformation ratio (T_R) and expulsion efficiency (f) are introduced to characterize the conversion degree of kerogen into hydrocarbons and the degree of expelled hydrocarbons to generated hydrocarbons, respectively, which are related to thermal maturity [19,36], as shown below.

$$T_R = \frac{1200 \times (HI_O - HI)}{HI_O \times (1200 - HI)} \quad (3)$$

$$f = 1 - \frac{HCI \times (1 - T_R)}{HI \cdot T_R} \quad (4)$$

According to Equations (3) and (4), the *TOCo* of source rocks can be obtained [19]:

$$TOCo = \frac{TOC}{1 - \alpha \times f \times T_R \times (1 - 1.2 \cdot TOC/100)} \quad (5)$$

where α is the ratio of the convertible carbon to the total carbon ($\alpha = HIo/1200 = GPIo/1200$).

Thus far, the data-driven HGE model of source rocks has been quantitatively established. When the source rocks reach the HGT, they begin to generate hydrocarbons, corresponding to an increase in the hydrocarbon index (*HCI*) and a decrease in the *HI* in the model (Figure 3b) [19], as shown in Equation (6). With an increase in the burial depth or thermal maturity, the source rocks begin to discharge hydrocarbons when they reach the HET, and the *GPI* begins to decrease. The residual hydrocarbon potential of source rocks is regarded as the residual *GPI* (*GPIr*):

$$HCI = GPI - HI \quad (6)$$

where $HCI = S_1/\text{TOC} \times 100$ represents the measured hydrocarbon index (mg HC/g TOC).

The hydrocarbon expulsion capacity (q_e) is determined by the *GPIo* and *GPIr*.

$$q_e = GPIo - GPIr \quad (7)$$

The hydrocarbon generation capacity (q_g) is the generated hydrocarbon per unit of TOC.

$$q_g = GPIo \quad (8)$$

The HGE intensities and amounts (I_g, I_e, Q_g, and Q_e) are obtained using Equations (9)–(12). The residual hydrocarbon amount (Q_r) is the difference between Q_g and Q_e, as shown in Equation (13):

$$I_g = \int_{Ro} 10^{-3} \cdot GPIo \cdot H \cdot \rho \cdot TOCo \cdot d(VRo) \quad (9)$$

$$I_e = \int_{Ro} 10^{-3} \cdot q_e \cdot H \cdot \rho \cdot TOCo \cdot d(VRo) \quad (10)$$

$$Q_g = \int_S \int_{Ro} 10^{-13} \cdot q_g \cdot H \cdot \rho \cdot TOC \cdot d(VRo) d(S) \quad (11)$$

$$Q_e = \int_S \int_{Ro} 10^{-13} \cdot q_e \cdot H \cdot \rho \cdot TOC \cdot d(VRo) d(S) \quad (12)$$

$$Q_r = Q_g - Q_e \quad (13)$$

where the unit of *GPIo*, *GPIr*, q_g, and q_e is mg HC/g TOC; the unit of I_g and I_e is 10^4 t/km^2; the unit of Q_g, Q_e, and Q_r is 10^8 t; H, S, and ρ are the thickness, area, and density of the source rocks, expressed as m, m^2, and g/cm^3, respectively; and *TOC* and *VRo* are expressed as %.

The Q_g can be classified into three types according to different accumulation dynamics and occurrence states: (a) After hydrocarbons are generated and expelled, they migrate to traps with a high porosity (Φ) and permeability (K) under buoyancy forces, forming conventional resources [37]. (b) After hydrocarbons are generated and expelled, they migrate to tight reservoirs with a low Φ and K under non-buoyancy forces (e.g., capillary force, overpressure), forming tight hydrocarbon resources. (c) Hydrocarbons are generated, and they remain in place, forming shale oil resources [38]. The buoyancy-driven hydrocarbon accumulation depth (BHAD) is defined as the dynamic boundary between conventional and unconventional tight hydrocarbon accumulation, which represents the critical conditions (Ro and depth) for the conversion of the accumulation dynamics from buoyancy to non-buoyancy forces [39]. The conventional reservoirs are formed above the BHAD, while the unconventional tight reservoirs are formed below the BHAD (Figure 3c).

4. Results and Discussion

4.1. Thickness of the Es4 Source Rocks

From bottom to top, as the sedimentary water gradually deepened, the distribution of the source rocks gradually expanded. As shown in Figure 4, the source rock thickness in the Es4n sub-member reaches 350 m (average = 120 m) and gradually decreases in the southward direction. Owing to the structural uplift and denudation in the north during the late Oligocene, the sedimentary centers of the Es4g and Es4d sub-members shifted from the north to the central part of the Niuxintuo area. The Es4g and Es4d source rocks are widely distributed, ranging from 50 to 500 m (average = 240 m) and from 20 to 420 m (average = 257 m), respectively.

4.2. OM Abundance

Here, the TOC contents and hydrocarbon generation potential (Pg = S_1 + S_2) are adopted to investigate the OM abundance of the Es4 source rocks (Table 1). The TOC contents of the Es4d, Es4g, and Es4n source rocks are mainly between 0.53–1.55%, 1.54–4.44%, and 2.11–5.18%, with averages of 1.00%, 3.09%, and 3.56%, respectively (Figure 5a). The Pg value of the Es4d source rock ranges from 0.45 to 4.23 mg HC/g rock, with an average of 1.49 mg HC/g rock. By contrast, the Pg values of the Es4g and Es4n source rocks are higher than 6 mg HC/g rock, with averages of 16.4 and 18.7 mg HC/g rock, respectively. The relationship between the TOC and Pg illustrates that the source rocks are poor to fair in the Es4d sub-member and good to excellent in the Es4g and Es4n sub-members (Figure 5b). Figure 6 shows the TOC distribution maps of the Es4 source rocks. The Es4d source rocks exhibit a limited area of TOC distribution, while the Es4g and Es4n source rocks show extensive TOC distribution ranges, whose OM abundance was generally concentrated in the central portion of the study area (Figure 6).

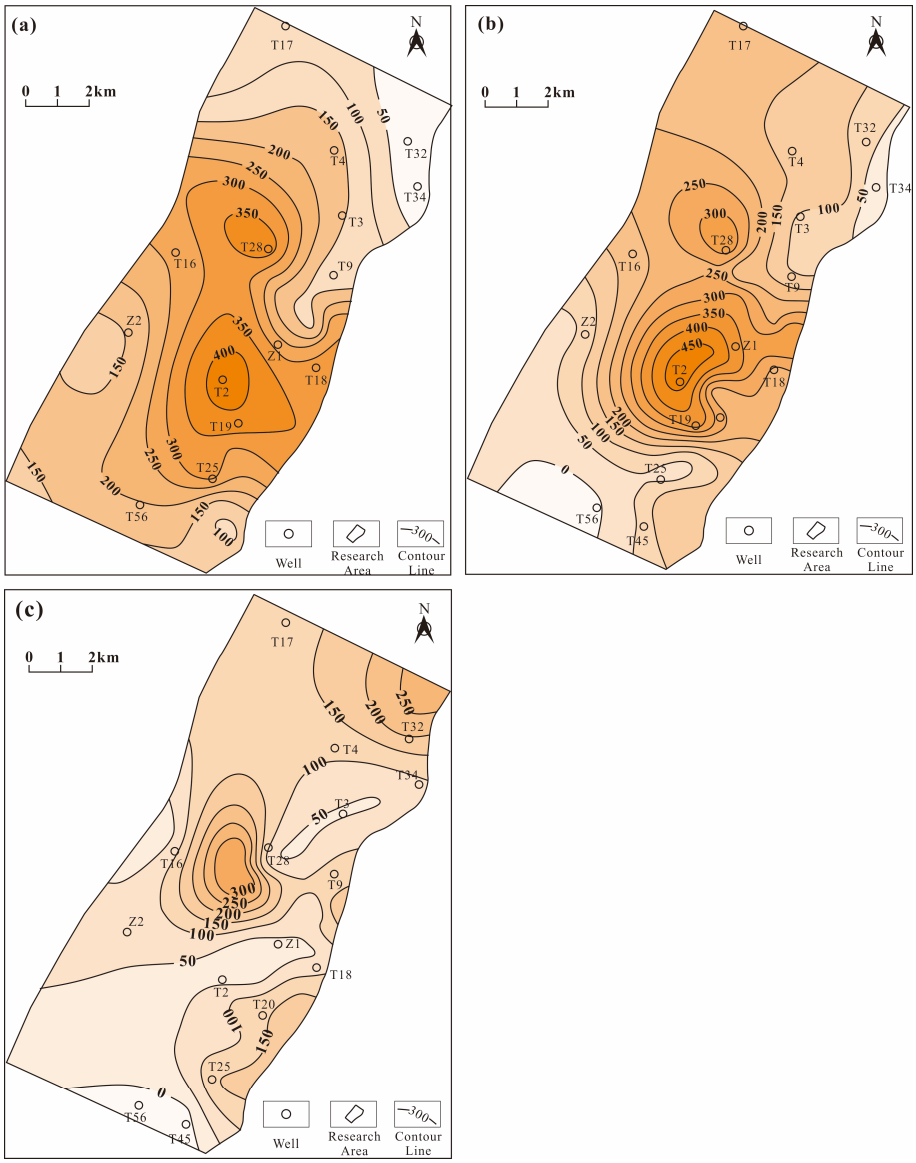

Figure 4. Thickness distribution map of the Es4 source rocks in the study area. (**a**) The Es4d source rocks; (**b**) The Es4g source rocks; (**c**) The Es4n source rocks.

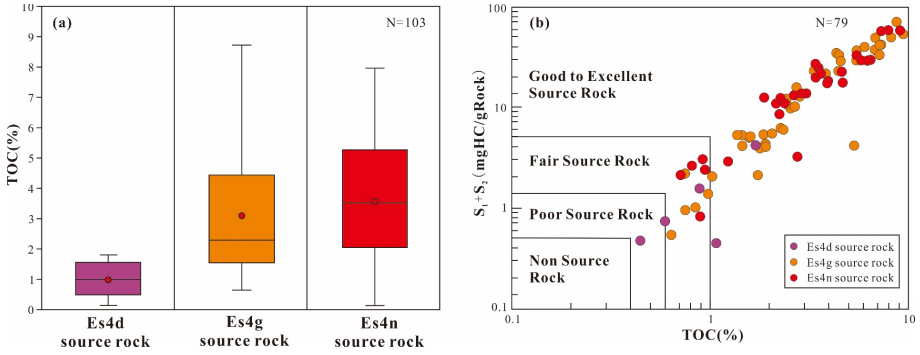

Figure 5. Source rock potential of the Es4d, Es4g, and Es4n source rocks in the Niuxintuo area. (**a**) TOC box plot. (**b**) (S_1 + S_2) vs. TOC plot.

Table 1. Rock-Eval pyrolysis data used in the study area.

Well	Depth (m)	Strata	*TOC* (%)	T_{max} (°C)	S_1 (mg *HC*/g rock)	S_2 (mg *HC*/g rock)	S_1+S_2 (mg/g rock)	HI (mg *HC*/g *TOC*)	*GPI* (mg *HC*/g *TOC*)	Well	Depth (m)	Strata	*TOC* (%)	T_{max} (°C)	S_1 (mg *HC*/g rock)	S_2 (mg *HC*/g rock)	S_1+S_2 (mg *HC*/g rock)	*HI* (mg *HC*/g *TOC*)	*GPI* (mg *HC*/g *TOC*)
T11	1690.0	Es4d	0.45	427	0.04	0.43	0.47	95.6	104.4	T1	2012.0	Es4n	5.56	439	0.66	33.08	33.74	595.0	606.8
T11	1716.0	Es4d	0.6	429	0.03	0.69	0.72	115.0	120.0	T12	1670.0	Es4n	0.72	438	0.06	2.06	2.12	286.1	294.4
T11	1720.0	Es4d	0.9	434	0.06	1.5	1.56	166.7	173.3	T12	1670.0	Es4n	0.95	437	0.1	2.3	2.40	242.1	252.6
Z1	1354.0	Es4d	1.09	430	0.01	0.44	0.45	40.4	41.3	T12	1690.7	Es4n	0.8	434	0.61	2.01	2.62	250.5	326.5
Z1	1367.0	Es4d	1.7	431	0.1	4.13	4.23	242.9	248.8	T14	1543.0	Es4n	7.96	430	0.88	57.68	58.56	724.6	735.7
Z1	1369.1	Es4d	12.4	435	0.83	21.54	22.37	173.7	180.4	T14	1546.8	Es4n	1.37	NA	NA	NA	NA	NA	NA
T1	1936.0	Es4g	1.56	438	0.07	5.02	5.09	321.8	326.3	T14	1588.5	Es4n	6.37	NA	NA	NA	NA	NA	NA
T1	1936.0	Es4g	1.46	435	0.13	5.24	5.37	358.9	367.8	T16	2490.0	Es4n	2.25	431	0.13	11.66	11.79	518.2	524.0
T1	1934.5	Es4g	3.82	441	0.37	21.28	21.65	557.1	566.8	T16	2490.0	Es4n	2.84	434	0.13	13.66	13.79	481.0	485.6
T11	2190.9	Es4g	2.78	434	0.35	12.98	13.33	467.0	479.5	T16	2378.0	Es4n	3.91	422	0.38	17.13	17.51	438.1	447.8
T11	2215.0	Es4g	4.42	436	0.38	23.48	23.86	531.0	539.8	T16	2378.0	Es4n	4.65	434	0.22	17.68	17.90	380.2	385.0
T12	1625.0	Es4g	7.18	435	0.25	33.04	33.29	460.2	463.7	T16	2378.0	Es4n	3.9	435	0.22	18.34	18.56	470.3	475.9
T12	1623.0	Es4g	5.57	432	0.89	36.2	37.09	649.9	665.9	T16	2377.2	Es4n	4.68	429	0.22	22.57	22.79	482.3	487.0
T12	1625.0	Es4g	5.99	434	0.45	39.52	39.97	659.8	667.3	T17	1216.5	Es4n	1.24	427	0.07	2.84	2.91	229.0	234.7
T12	1626.5	Es4g	7.14	442	0.59	40.61	41.20	568.8	577.0	T17	1071.5	Es4n	3.06	433	0.39	13.46	13.85	439.9	452.6
T12	1621.3	Es4g	8.03	442	1.14	49.87	51.01	621.1	635.2	T19	2726.0	Es4n	3.05	NA	NA	NA	NA	NA	NA
T12	1622.5	Es4g	8.73	444	0.52	70.2	70.72	804.1	810.1	T20	2740.5	Es4n	5.14	NA	NA	NA	NA	NA	NA
T16	2204.5	Es4g	2.06	424	0.16	5.27	5.43	255.8	263.6	T22	1683.0	Es4n	3.53	NA	NA	NA	NA	NA	NA
T16	2205.0	Es4g	2.3	437	0.13	6.02	6.15	261.7	267.4	T24	1583.7	Es4n	0.22	NA	NA	NA	NA	NA	NA
T16	2205.0	Es4g	2.27	436	0.1	6.19	6.29	272.7	277.1	T25	2494.6	Es4n	2.79	441	0.03	3.16	3.19	113.3	114.3
T19	2485.9	Es4g	0.97	438	0.02	1.39	1.41	143.3	145.4	T25	2304.4	Es4n	1.9	432	0.24	12.54	12.78	660.0	672.6
T19	2390.0	Es4g	1.04	438	0.09	1.97	2.06	189.4	198.1	T25	2504.8	Es4n	1.05	NA	NA	NA	NA	NA	NA
T19	2390.0	Es4g	0.73	440	0.13	2.01	2.14	275.3	293.2	T25	2304.0	Es4n	2.02	NA	NA	NA	NA	NA	NA
T19	2492.0	Es4g	1.88	439	0.11	4.17	4.28	222.0	227.7	T25	2304.0	Es4n	3.28	NA	NA	NA	NA	NA	NA
T19	2492.0	Es4g	1.88	439	0.12	4.36	4.48	231.9	238.3	T25	2302.6	Es4n	3.68	NA	NA	NA	NA	NA	NA
T20	2485.0	Es4g	0.76	439	0.11	0.83	0.94	109.2	123.7	T25	2306.1	Es4n	4.36	NA	NA	NA	NA	NA	NA
T20	2483.0	Es4g	0.84	439	0.07	0.93	1.00	110.7	119.1	T25	2304.4	Es4n	5.31	NA	NA	NA	NA	NA	NA
T20	2345.0	Es4g	1.58	435	0.11	5.01	5.12	317.1	324.1	T27	2506.1	Es4n	6.12	NA	NA	NA	NA	NA	NA
T20	2345.0	Es4g	1.36	434	0.16	5.18	5.34	380.9	392.7	T28	1870.5	Es4n	0.13						
T28	1785.2	Es4g	2.42	424	0.26	10.64	10.90	439.7	450.4	T3	1030.0	Es4n	7.38	435	0.83	56.12	56.95	760.4	771.7
T28	1787.6	Es4g	6.94	434	0.46	48.86	49.32	704.0	710.7	T4	1279.7	Es4n	2.14	432	0.17	10.66	10.83	498.1	506.1
T3	1000.5	Es4g	1.49	429	0.18	4.01	4.19	269.1	281.2	T5	1643.0	Es4n	0.9	431	0.06	0.76	0.82	84.4	91.1
Z1	1477.0	Es4g	0.64	436	0.01	0.53	0.54	82.8	82.8	T5	1639.0	Es4n	3.51	439	0.19	22.62	22.81	644.4	649.9
Z1	1576.3	Es4g	1.75	433	0.04	2.04	2.08	116.6	118.9	T5	1639.0	Es4n	3.42	441	0.23	25.46	25.69	744.4	751.2
Z1	1475.2	Es4g	1.76	443	0.25	3.71	3.96	211.0	225.3	Z1	1862.0	Es4n	0.92	438	0.05	2.88	2.93	313.0	318.5
Z1	1576.5	Es4g	5.37	423	0.04	4.11	4.15	76.5	77.3	Z1	1834.7	Es4n	2.25	433	0.19	8.39	8.58	372.9	381.3
Z1	1725.5	Es4g	1.88	435	0.09	5.33	5.42	283.5	288.3	Z1	1832.0	Es4n	2.66	438	0.15	12.73	12.88	478.6	484.2

Table 1. *Cont.*

Well	Depth (m)	Strata	*TOC* (%)	T_{max} (°C)	S_1 (mg *HC*/g rock)	S_2 (mg *HC*/g rock)	S_1+S_2 (mg/g rock)	HI (mg *HC*/g *TOC*)	*GPI* (mg *HC*/g *TOC*)	Well	Depth (m)	Strata	*TOC* (%)	T_{max} (°C)	S_1 (mg *HC*/g rock)	S_2 (mg *HC*/g rock)	S_1+S_2 (mg *HC*/g rock)	*HI* (mg *HC*/g *TOC*)	*GPI* (mg *HC*/g *TOC*)
Z1	1765.5	Es4g	2.55	434	0.21	9.74	9.95	382.0	390.2	Z1	1858.2	Es4n	3.66	436	0.45	20.46	20.92	559.0	571.6
Z1	1767.0	Es4g	2.6	440	0.82	9.69	10.51	372.3	403.8	Z1	1904.4	Es4n	8.95	441	1.55	56.34	57.89	629.6	646.9
Z1	1767.5	Es4g	2.45	437	0.17	11.91	12.08	486.1	493.1	Z1	1841.0	Es4n	0.71	NA	NA	NA	NA	NA	NA
Z1	1786.2	Es4g	2.76	434	0.29	15.28	15.58	553.6	564.5	Z1	1837.0	Es4n	2.34	NA	NA	NA	NA	NA	NA
Z1	1792.4	Es4g	3.35	439	0.28	22.66	22.94	676.4	684.8	Z1	1842.5	Es4n	3.64	NA	NA	NA	NA	NA	NA
Z1	1809.6	Es4g	4.5	437	0.41	28.34	28.77	629.8	639.3	Z1	1840.0	Es4n	3.87	NA	NA	NA	NA	NA	NA
Z1	1766.0	Es4g	5.6	442	0.57	29.73	30.30	530.9	541.1	Z1	1839.0	Es4n	4.92	NA	NA	NA	NA	NA	NA
Z1	1815.3	Es4g	4.42	445	0.68	31.57	32.25	714.9	730.3	Z1	1847.0	Es4n	5.38	NA	NA	NA	NA	NA	NA
Z1	1815.3	Es4g	4.36	445	0.85	32.41	33.26	743.9	763.4	Z1	1843.0	Es4n	6.51	NA	NA	NA	NA	NA	NA
Z1	1813.9	Es4g	6.83	438	0.62	36.88	37.50	540.0	549.1	Z1	1842.0	Es4n	6.73	NA	NA	NA	NA	NA	NA
Z1	1792.9	Es4g	7.18	444	0.51	40.84	41.35	568.8	575.9	Z1	1831.2	Es4n	2.39	443	0.39	10.64	11.03	444.4	460.7
Z1	1802.0	Es4g	9.4	437	2.33	52.6	54.93	559.8	584.6	NA	NA	NA	NA	NA	NA	NA	NA	NA	NA
T1	1967.4	Es4n	3.37	438	0.59	19.4	19.99	575.3	592.8	NA	NA	NA	NA	NA	NA	NA	NA	NA	NA
T1	2020.3	Es4n	6	437	0.49	29.25	29.74	487.5	495.7	NA	NA	NA	NA	NA	NA	NA	NA	NA	NA
T1	1968.0	Es4n	5.72	440	0.57	29.72	30.29	519.6	529.6	NA	NA	NA	NA	NA	NA	NA	NA	NA	NA
T1	2012.0	Es4n	6.34	441	0.21	30.54	30.75	481.7	485.0	NA	NA	NA	NA	NA	NA	NA	NA	NA	NA

NA: Not available.

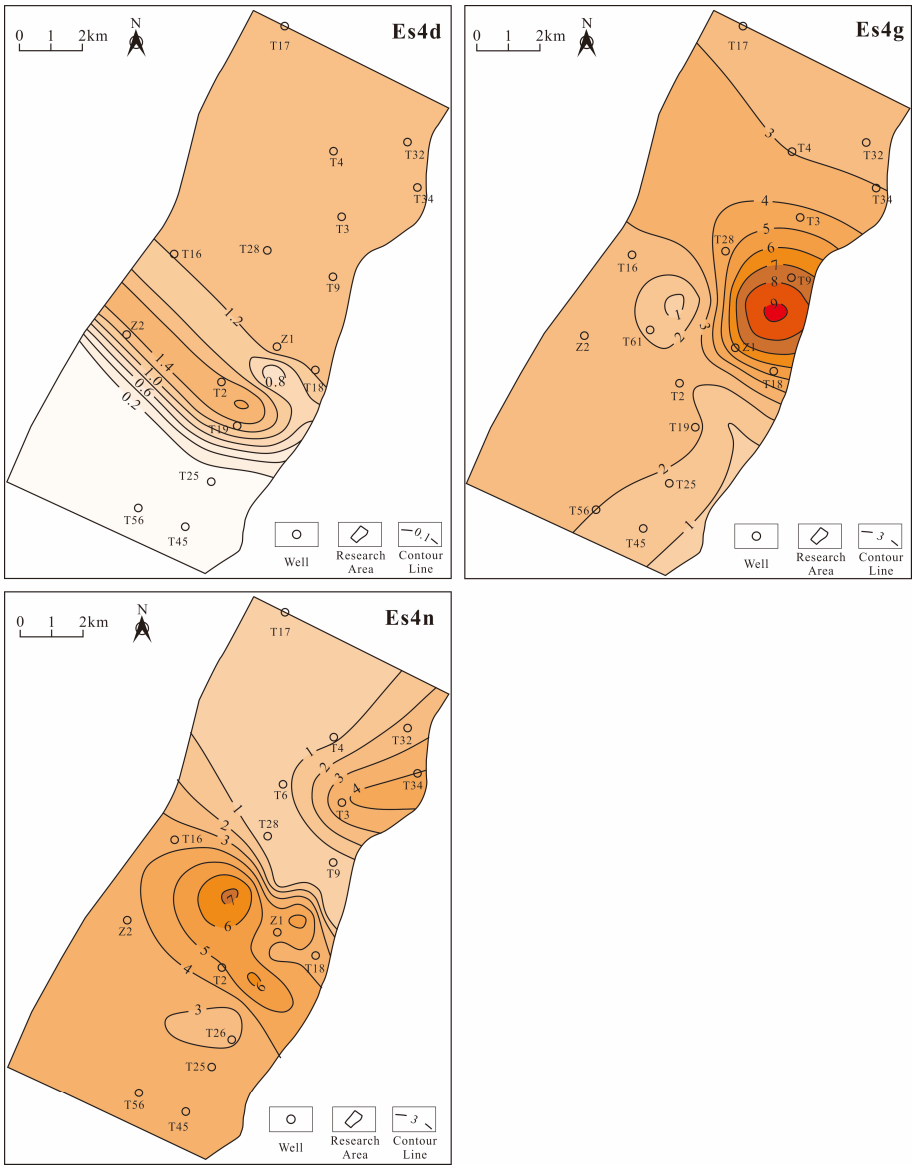

Figure 6. TOC distribution maps of the Es4d, Es4g, and Es4n source rocks in the Niuxintuo area.

4.3. OM Type

The maceral analysis of the Es4 source rocks shows that the OM is mainly composed of liptinite. Telalginite appears as translucent strips or clumps with a strong yellow-green fluorescence (Figure 7a). Lamalginite is generated from algae, always being oriented parallel to bedding planes, and presents with a mat-like shape (Figure 7b). Bituminite is the decomposition product of aquatic organisms and algae and shows a green-yellow fluorescence (Figure 7c). In addition, a dark brown irregular mineral–bituminite matrix can be observed (Figure 7a,c,d).

The OM type in the Liaohe Western Depression is considered as type I–II_1 [40,41]. Figure 8 shows that the HI value of the Es4 source rocks ranges from 77 to 804 mg/g, and the T_{max} ranges from 420 °C to 450 °C. The hydrocarbon group components of the Es4 source rocks mainly comprise asphaltene and non-hydrocarbons (40%–62%) and saturated hydrocarbons (24%–45%), indicating the presence of type II kerogen (Figure 8b). Overall, the kerogen of the Es4 source rocks is mainly type II (accounting for 73%), with some parts being type I (accounting for 22%).

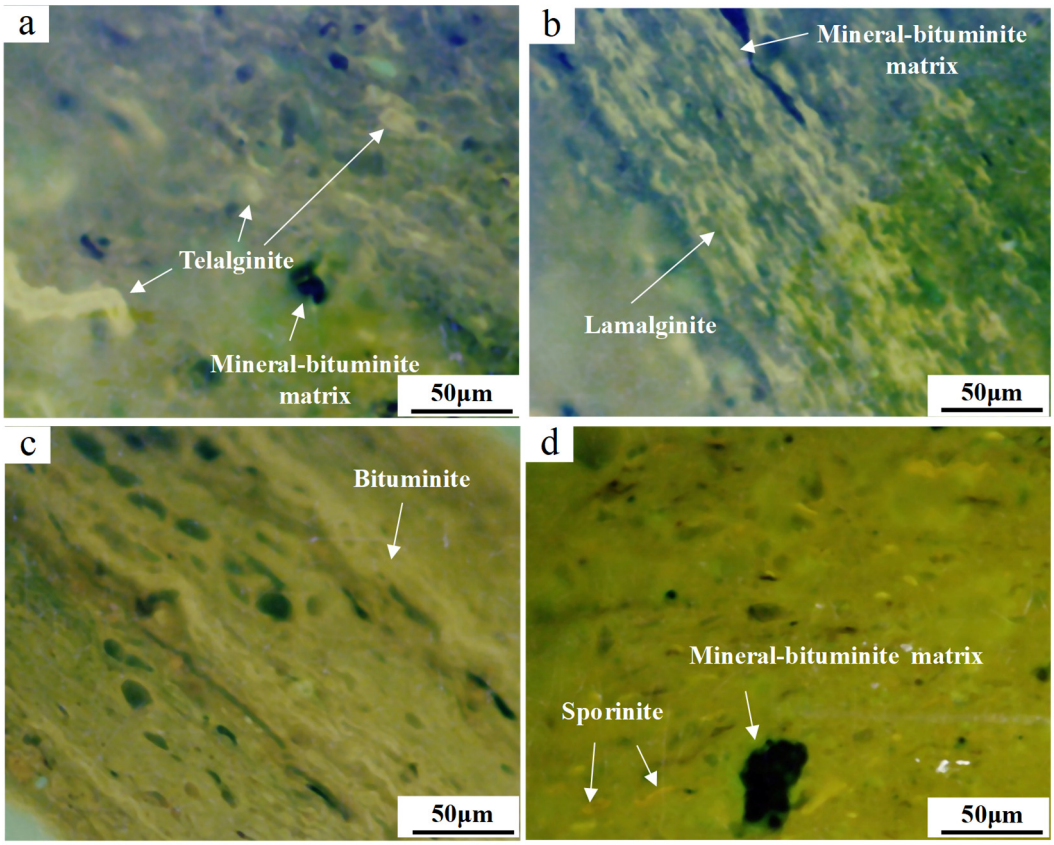

Figure 7. Photomicrographs showing maceral groups of the Es4 source rocks in the Niuxintuo area. (**a**) Brightly fluorescent telalginite and mineral–bituminite matrix, 1450 m, mudstone, ×500. (**b**) Brightly fluorescent lamalginite and mineral–bituminite matrix, 1430 m, mudstone, ×500. (**c**) Bituminite, 1200 m, mudstone, ×500. (**d**) Sporinite and mineral–bituminite matrix, 1200 m, mudstone, ×500.

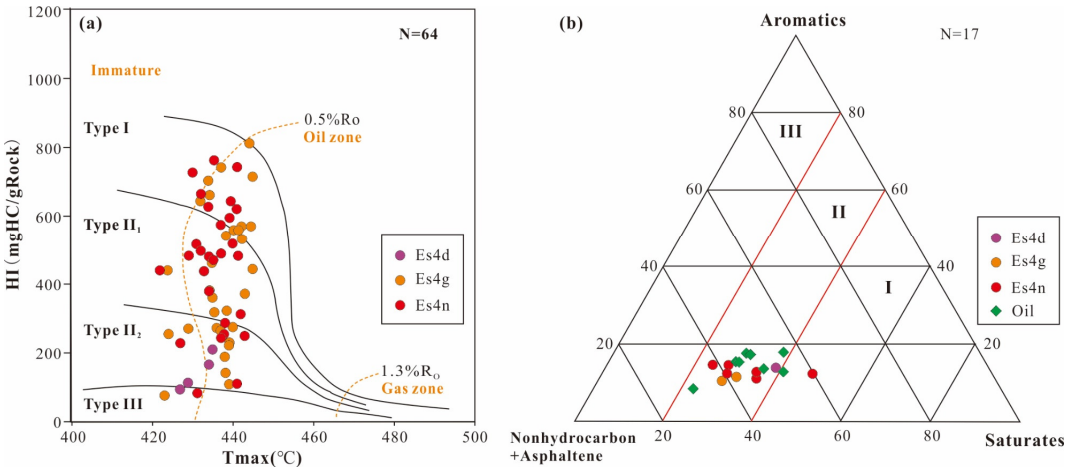

Figure 8. Classification plots of the Es4d, Es4g, and Es4n source rock types in the Niuxintuo area. (**a**) Cross plots of T_{max} versus HI. (**b**) Triangle diagram of the hydrocarbon group components.

4.4. Thermal Maturity

In this study, VRo, T_{max}, and biomarker parameters were adopted to assess the thermal maturity of source rocks. Figure 9a shows that the VRo values of the Es4 sub-member range from 0.26% to 0.63% (with corresponding depths of < 2500 m). However, a higher VRo value (0.88%) was found for the shallow-buried Mesozoic mudstone sample, mainly

due to the regional tectonic uplift in the late Oligocene. The average T_{max} values of the Es4d, Es4g, and Es4n source rocks are 431, 437 and 435 °C, respectively (Figure 9b). Steranes C_{29}20S/(20S + 20R) and $C_{29}\alpha\beta\beta/(\alpha\beta\beta + \alpha\alpha\alpha)$ are often used to assess thermal maturity [42,43]. The C_{29}20S/(20S + 20R) of the Es4 source rocks is 0.24–0.37 (with an average of 0.12), and the $C_{29}\alpha\beta\beta/(\alpha\beta\beta + \alpha\alpha\alpha)$ is 0.24–0.37 (with an average of 0.29), suggesting that the source rocks are in an early mature stage (Figure 9c,d). Overall, the Es4n and Es4g source rocks are in the low-mature to mature stage, while the Es4d source rocks are in the immature to low-mature stage.

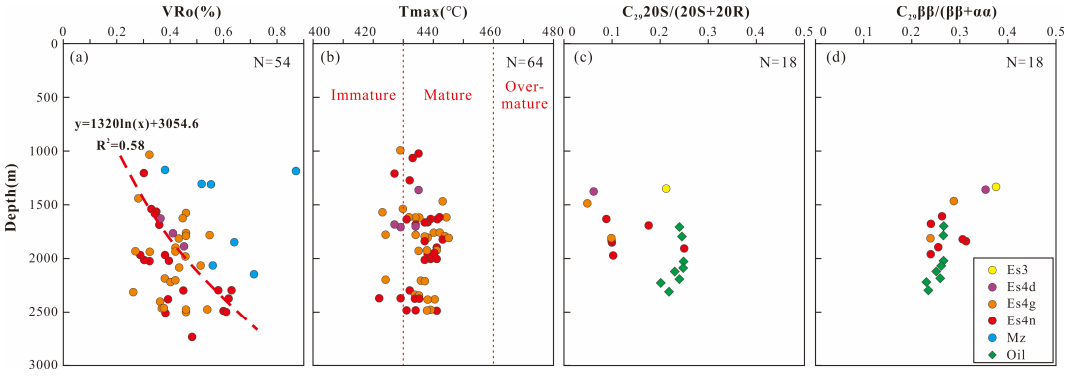

Figure 9. Thermal maturity of source rocks in the Niuxintuo area. (**a**) Ro. (**b**) T_{max}. (**c**) C_{29}20S/(20S + 20R). (**d**) $C_{29}\alpha\beta\beta/(\alpha\beta\beta + \alpha\alpha\alpha)$.

4.5. Hydrocarbon Generation Simulation of Low-Maturity Source Rocks

Five low-maturity source rock samples were collected from the Liaohe Western Depression to conduct the thermal simulation experiment. Table 2 illustrates the maceral groups and kerogen types of the five low-maturity samples, which have similar deposition environments to the Es4 source rocks in the Niuxintuo area. Variations in the geochemical parameters of the five simulated samples are shown in Figure 10. The measured VRo values have an exponential fitting relationship with the experiment temperature (Figure 10a). With the increase in thermal maturity, the TOC contents of the type I and II_1 samples decrease significantly from 6.43% to 2.42% and from 3.84% to 2.01%, respectively (Figure 10b). The TOC contents of the type II_2 and III samples decrease from 2.0%, 3.3%, and 1.9% to 1.6%, 2.6%, and 1.5%, respectively. In the thermal simulation, the initial T_{max} values of the type I–III samples are 421–429 °C and then increase to 456–512 °C (Figure 10c). Before VRo < 0.78%, the Pg and HI decrease slowly (Figure 10d,e). As the thermal maturity increases (VRo > 0.78%), the Pg and HI decrease rapidly, especially for the type I and type II kerogens. The HCI values of the type I–III samples decrease before VRo = 0.5% and then increase rapidly, showing that a large number of hydrocarbons are generated (Figure 10f). When VRo is > 0.78%, the HI values decrease rapidly because of the hydrocarbons' expulsion. Moreover, the slight variations in the geochemical parameters of the type II_2 and III samples with increasing thermal maturity lead to a lower hydrocarbon generation potential than that of the type I and II_1 samples.

The rates of hydrocarbon generation, expulsion, and retention and their variations during the thermal simulation are illustrated in Figure 11. When VRo = 0.3%, retention oil is present in the low-maturity simulated samples. With the increase in VRo to 0.5%, the hydrocarbon generation (total hydrocarbon) rate and retention rate exhibit a slight decreasing trend, while the oil expulsion rate of the type I–III source rocks increases from 0 to 1.5, 11.86, 3.58, 2.74, 1.01, and 0.09, respectively, suggesting that the shale samples discharge a small amount of oil. As the thermal maturity continually increases, the hydrocarbon generation, expulsion, and retention rates increase rapidly. When VRo = 0.78%, the hydrocarbon retention rates of the type I and II samples show a peak value, while the hydrocarbon retention rate of the type III shale peaks at VRo = 0.95%. The inflection point of the hydrocarbon retention rate corresponds to the onset of the rapid increase in the

hydrocarbon expulsion rate, which means that large amounts of hydrocarbons are expelled. When VRo is > 1.1%, the oil expulsion rates of the type I–II samples display a decreasing trend after reaching the peak value, and their hydrocarbon retention rates continue to decrease. The gas expulsion rates of the type I–III samples continue to increase, mainly because of the cracking of the kerogen and oil. For the type I and II samples, the variation trend of the hydrocarbon generation rate is consistent with the oil expulsion rate, while for the type III samples, the hydrocarbon generation rate is consistent with the gas expulsion rate, indicating that the type III shale has good gas generation potential.

Table 2. Maceral groups of simulated samples.

Sample ID	Lithology	Maceral Analysis					Kerogen Type
		Vitrinite	Inertinite	Exinite	Liptinite		
					Alginite	Bituminite	
D16	Shale	7	<2	0	7	84	I
D22	Calcareous shale	9	<1	1.5	5.5	83	II_1
G25	Shale	8	<1	2	2	87	II_2
S499	Shale	14	<1	6	/	79	II_2
S101	Mudstone	4	<2	36	/	58	III

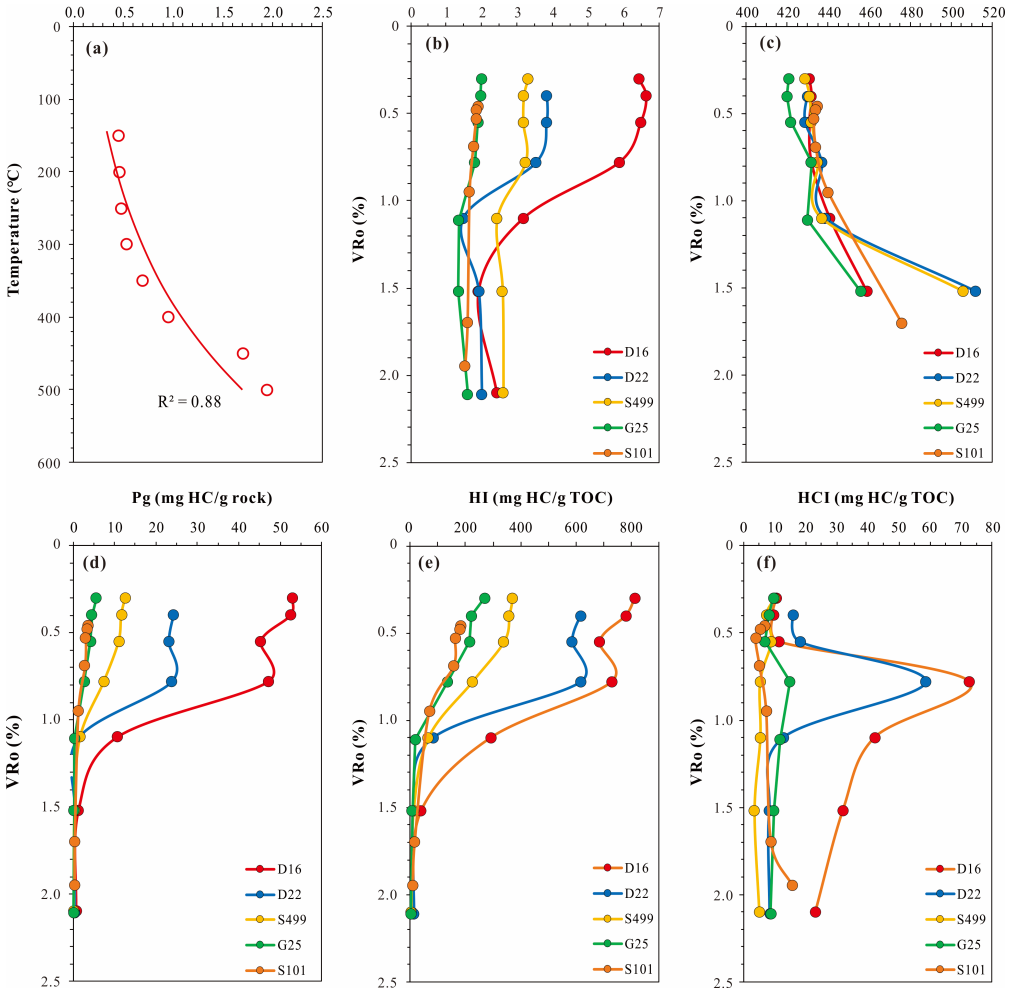

Figure 10. The evolution of geochemical parameters with increasing thermal maturity in the hydrocarbon generation simulation experiment. (**a**) Thermal simulation temperature vs. thermal maturity. (**b**–**f**) Geochemical parameters vs. thermal maturity.

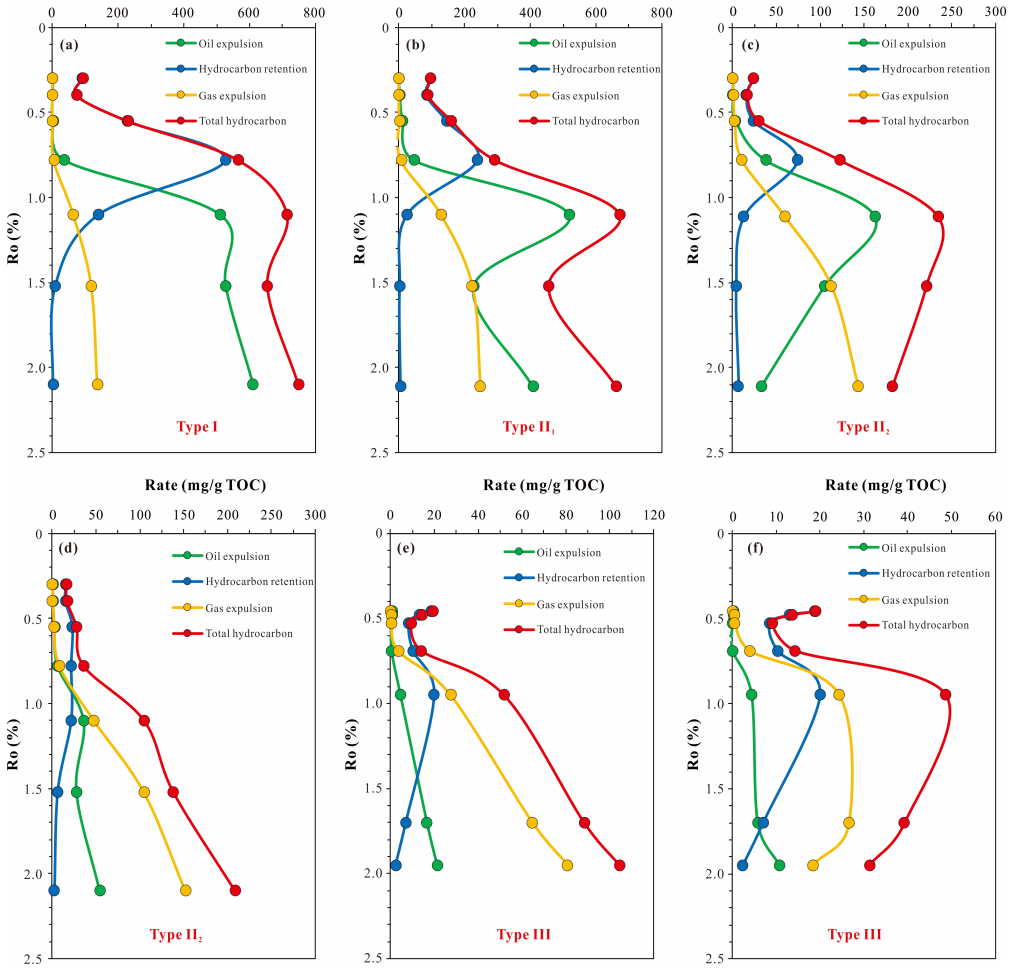

Figure 11. Variations in the hydrocarbon production rate with an increase in thermal maturity of the Es4 source rocks. (**a**) D16; (**b**) D22; (**c**) G25; (**d**) S499; (**e**) S101; (**f**) S101 (Parallel experiment).

4.6. Optimal Regression Relationship Based on Rock-Eval/TOC Datasets

Considering the low maturity of the Es4 source rocks in the study area, the Rock-Eval pyrolysis and VRo data of mature source rocks and the five simulated shales in the Liaohe Western Depression were also adopted to ensure that the datasets were distributed in a complete thermal maturity sequence. Using numerical analysis, the optimal fitting curves and 95% confidence bands of GPI, HI, and VRo were quantitatively characterized (Figure 12). For the type II source rocks (containing a certain amount of type I kerogen) in the study area, the optimal fitted GPI and HI curves exhibit positive relationships with the measured GPI and HI values, and the correlation coefficient (R^2) reaches 0.7. In the regression model, the GPIo and HIo of the Es4 source rocks are 600 mg HC/g TOC (Figure 12a,c). The β_1 and β_2 of the Es4 source rocks are 0.55%VRo and 0.62%VRo, respectively, which correspond to the thermal maturity observed when large amounts of hydrocarbons are generated and discharged from source rocks. The residual histograms of GPI and HI show a normal distribution, indicating the reliability of the regression relationship (Figure 12b,d).

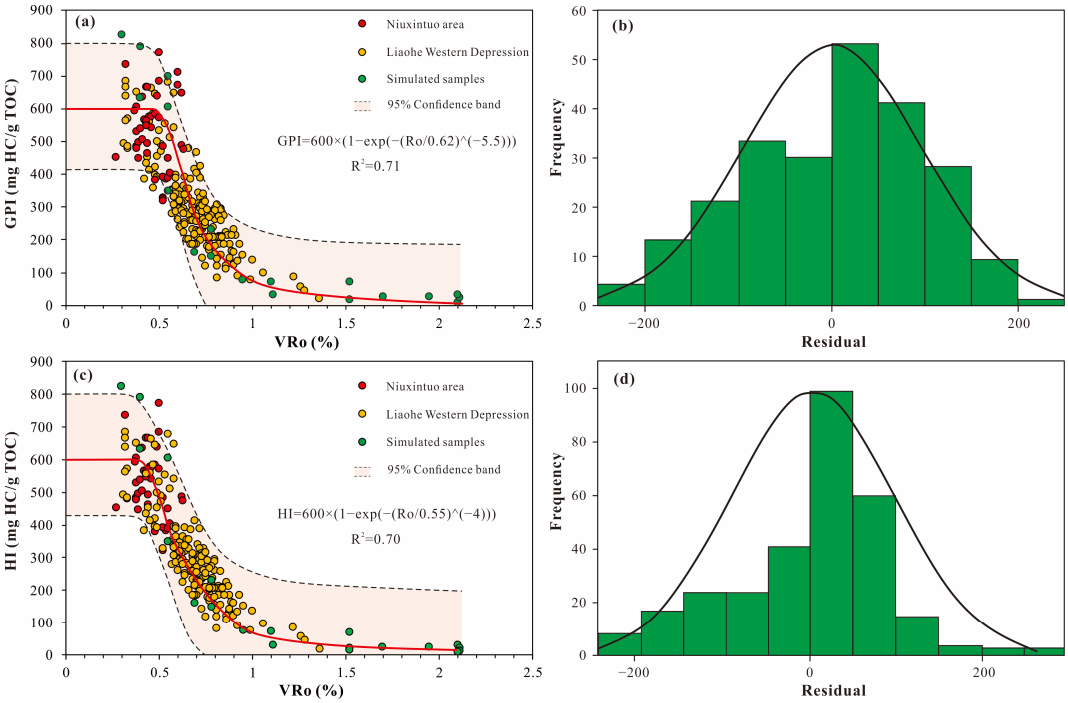

Figure 12. The fitted model of Rock-Eval data and VRo using the data-driven approach. (**a**) GPI vs. Ro. (**b**) Residual histogram of GPI-Ro. (**c**) HI vs. Ro. (**d**) Residual histogram of HI-Ro.

5. Discussion

5.1. Optimized HGE Model

The HGE models established using the traditional method and the data-driven method proposed in this study were observed and compared visually (Figure 13) [12]. As shown in Figure 13a, the GPIo is 820 mg HC/g TOC, which was determined by the hand-drawn maximum envelope of the dataset. The HET corresponds to the thermal maturity of 0.43% when the GPI begins to decrease. However, the HGT could not be adopted as 0.5% VRo, which would lead us to the fallacy that hydrocarbons are expelled before they are generated. The residual GPI (GPIr) exhibits a rapid decrease with increasing thermal maturity, which is excessively reduced by 75% when the VRo is 0.6%–0.7%. Based on the regression relationships of GPI, HI, and VRo, the optimized model was quantitatively established using numerical analysis to investigate the HGE characteristics of the Es4 source rocks (Figure 13b). The GPIo and HIo of the Es4 source rocks are 600 mg HC/g TOC. When VRo = 0.36%, the HI begins to decrease, and HCI starts to appear, which means that hydrocarbon generation commences. The HGT and HET of the Es4 source rocks are determined to be 0.36%VRo and 0.46%VRo, respectively. The organic material (bacteria andalgae) in the saline sedimentary environment provides a favorable material basis for the HGE from source rocks of a lower maturity [44].

5.2. Application in the Low-Mature to Mature Source Rocks

The onset of hydrocarbon generation has been discussed for decades, and it can be concluded that the oil generation stage of low-maturity source rocks approximately corresponds to VRo = 0.2%–0.7% or 0.3%–0.6% [45–47]. The hydrogen-rich organic maceral and reductive hypersaline paleoenvironment is considered to provide the indispensable conditions for the hydrocarbon generation of low-maturity source rocks [48–50]. The relationship between the Pr/n-C_{17} and Ph/n-C_{18} of the Es4 source rocks and crude oil indicates a reducing sedimentary environment and a gradual decrease in the thermal maturity of the source rocks (Figure 14).

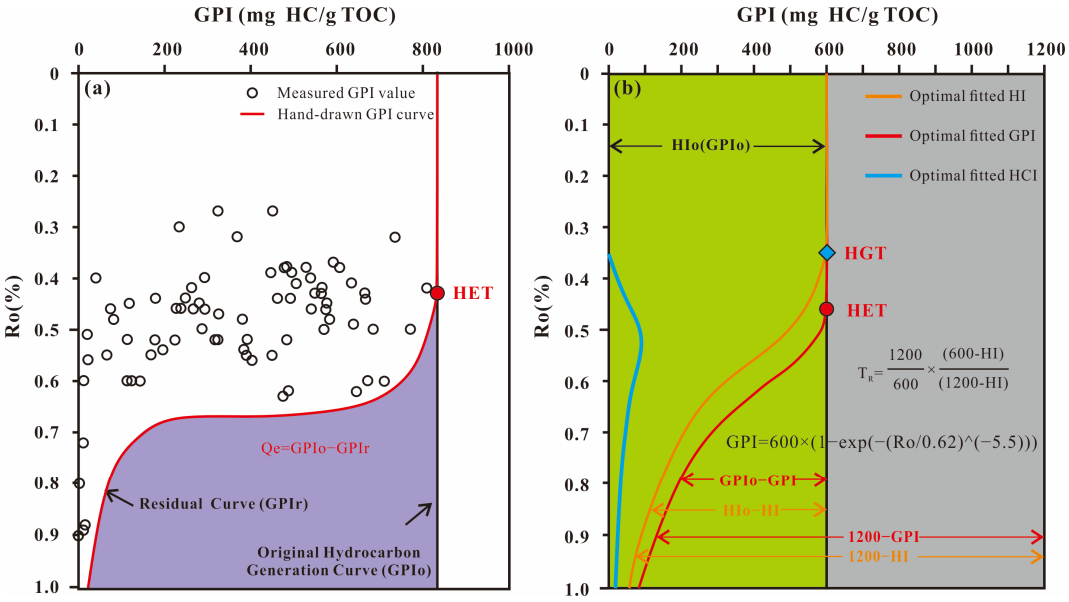

Figure 13. Comparison between the traditional HGE model (**a**) and the quantitative optimized model (**b**) of the Es4 source rocks in the Niuxintuo area.

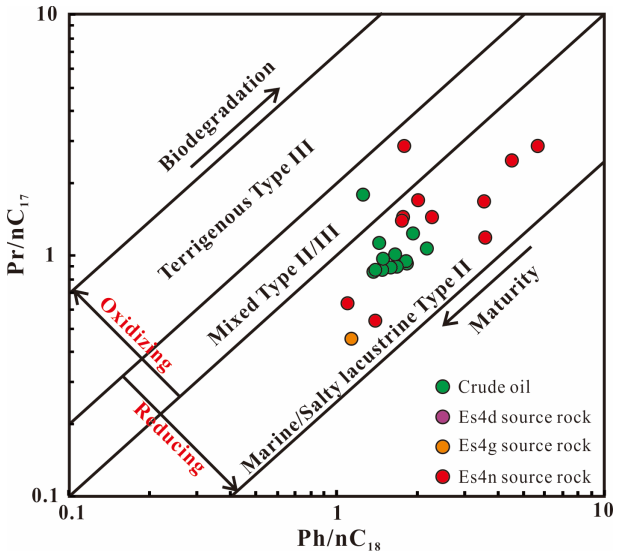

Figure 14. Plot of Pr/*n*-C_{17} vs. Ph/*n*-C_{18} showing the sedimentary environment and thermal maturity.

The hydrocarbon generation of source rocks leads to a decrease in TOC [19,36]. The hydrocarbon resource potentials calculated using the measured TOC and the restored TOCo show considerable differences [16]. Compared with the TOC distribution, the TOCo contents increase significantly with increasing thermal maturity (Figure 15). Based on the TOCo, GPIo, effective thickness, and density of the Es4 source rocks, the I_g and I_e were obtained (Figure 16). The maximum I_g values of the Es4d, Es4g, and Es4n source rocks could reach 1.00×10^7, 4.00×10^7, and 3.20×10^7 t/km^2, respectively, indicating their prospective hydrocarbon generation potential. The I_g value of the Es4n source rock was distributed throughout almost all of the study area, except for the southernmost area. The maximum I_e values of the Es4d, Es4g, and Es4n source rocks could reach 3.00×10^7, 2.60×10^6, and 5.00×10^6 t/km^2, respectively. By contrast, the distribution range of I_e was more limited than that of I_g. Similarly, the Q_g of the Es4 source rocks in the study area was considerable, while the Q_e was limited. The Q_g values of the Es4d, Es4g, and Es4n source rocks were 3.99×10^8, 11.42×10^8, and 7.02×10^8 t, respectively. In the Es4d and Es4g

sub-members, the limited hydrocarbon expulsion ranges led to a small Q_e (2.50×10^6 and 2.10×10^7 t). By contrast, the expulsion amount reached 1.09×10^8 t in the case of the Es4n source rocks.

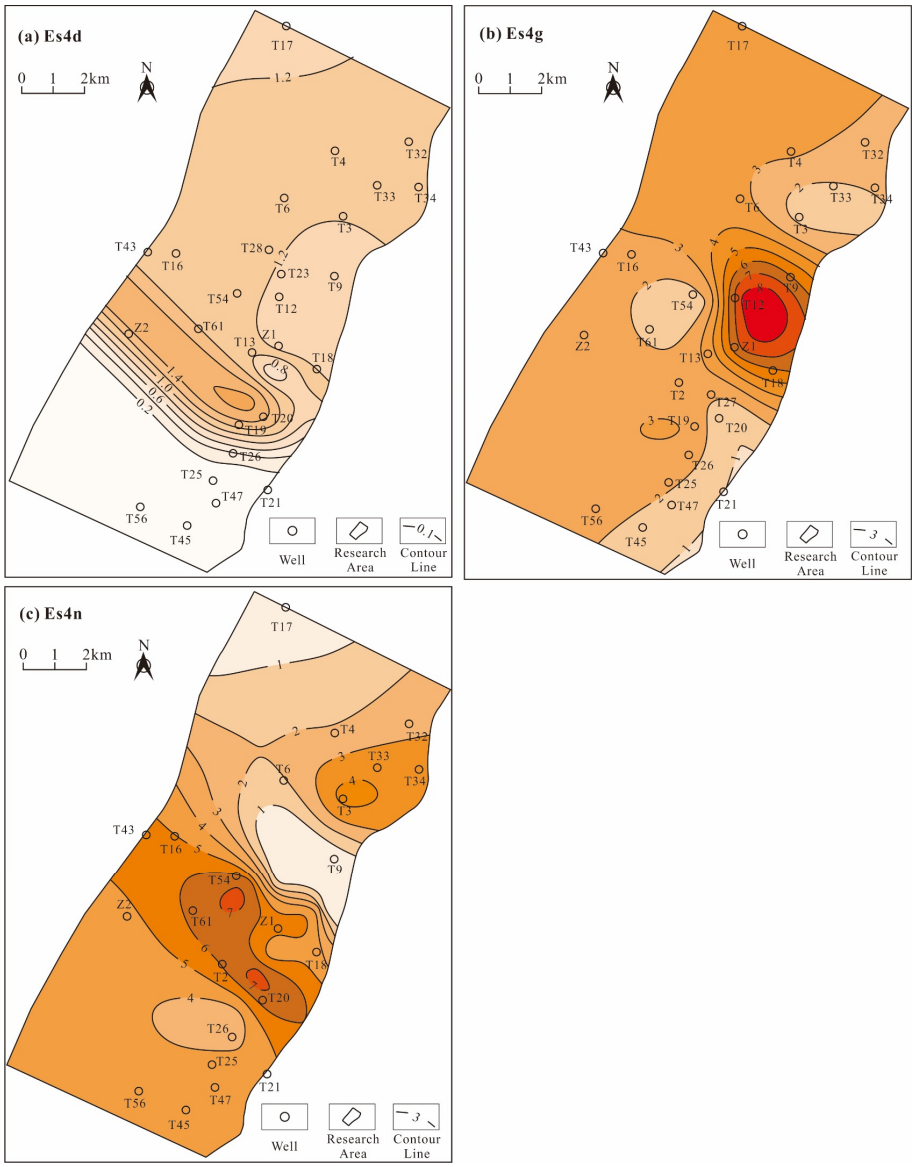

Figure 15. Distribution of the restored TOCo of the Es4 source rocks in the Niuxintuo area. (**a**) The ES4d source rocks; (**b**) The ES4g source rocks; (**c**) The ES4n source rocks.

Pang et al. [51] proposed the dynamic field division of conventional and unconventional hydrocarbon enrichments based on statistical analysis, reservoir anatomy, and physical simulation experiments. The BHAD was considered as the boundary of conventional and unconventional tight hydrocarbon reservoirs, corresponding to a porosity of 10% and permeability of 1 mD [39,51–53]. Figure 17 shows the variations in porosity with the burial depth and oil–water distribution in a profile of the study area. The burial depth and VRo value corresponding to the BHAD were determined to be 2180 m and 0.56%, respectively.

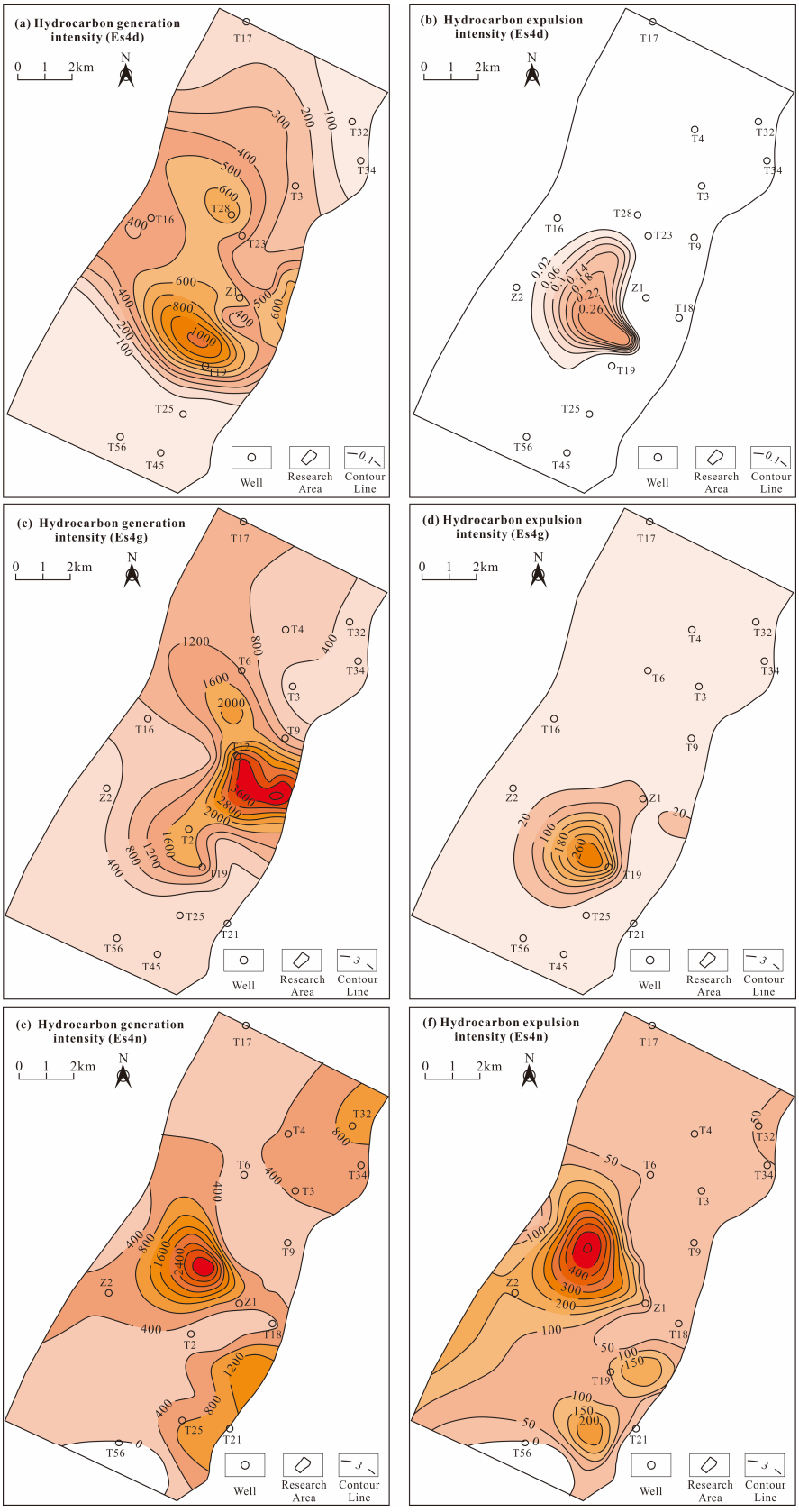

Figure 16. The I_g and I_e distributions of the Es4 source rocks in the Niuxintuo area. (**a**) I_g of the Es4d source rocks; (**b**) I_e of the Es4d source rocks; (**c**) I_g of the Es4g source rocks; (**d**) I_e of the Es4g source rocks; (**e**) I_g of the Es4n source rocks; (**f**) I_e of the Es4n source rocks.

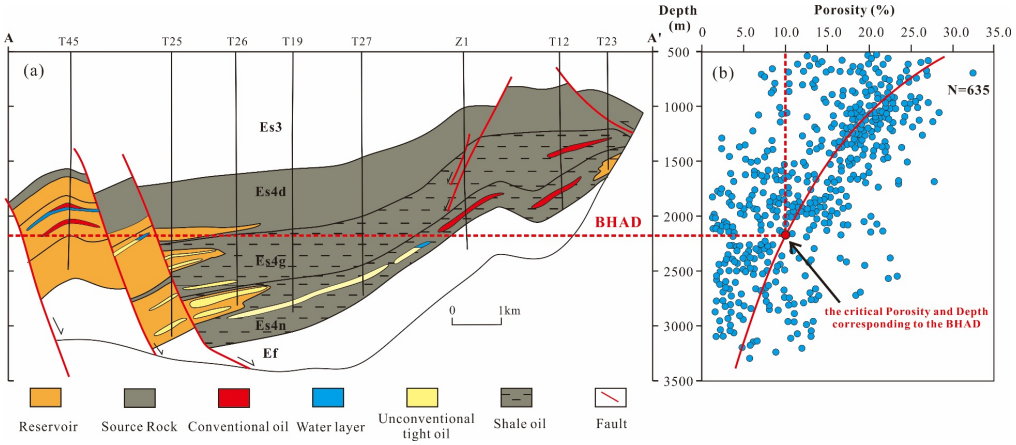

Figure 17. Determination of the BHAD in the Niuxintuo area. (**a**) Hydrocarbon reservoir profile. (**b**) Variation in porosity with burial depth.

For the Es4n source rock, the conventional oil potential between the HET and BHAD is 3.20 × 10^7 t (Figure 18). Below the BHAD, the tight oil potential is 7.70 × 10^7 t. The residual hydrocarbon calculated using Equation (13) is the shale oil potential, which could reach 5.93 × 10^8 t. Considering the processes of hydrocarbon migration, accumulation, preservation, or destruction, it is necessary to use the appropriate accumulation coefficient. The adjacent source–reservoir conditions in the study area lead to a greater accumulation coefficient. In this study, 30%, 45%, and 54% were adopted as the accumulation coefficients of three kinds of resources, respectively [51]. In the Es4n sub-member, the conventional, unconventional tight, and shale oil resources are 1.00 × 10^7, 3.50 × 10^7, and 3.20 × 10^8 t, respectively. In the Es4g sub-member, the shale oil resource is 6.05 × 10^8 t. In general, the conventional oil resources in the Niuxintuo area are relatively limited. The exploration of unconventional tight oil resources should focus on the Es4n sub-member, while the exploration of shale oil should focus on the Es4g and Es4n sub-members.

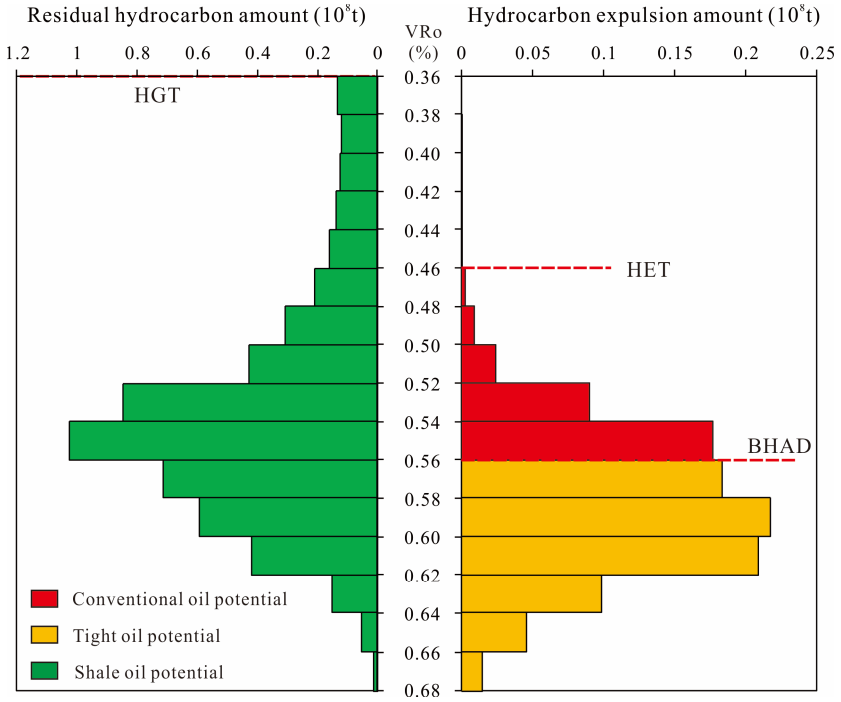

Figure 18. Conventional, unconventional tight, and shale oil resource potentials of the Es4n source rocks in the Niuxintuo area.

5.3. Limitations

In this study, due to the limited geochemical data on mature to high-mature source rocks, the R^2 of the regression model was only 0.7, and differences in the HGE characteristics of different types of source rocks were not studied in more detail. In a further study, we will conduct more intensive sampling and geochemical analyses of the Es4 source rocks to supplement the datasets and improve the R^2 of the regression model. We suggest that researchers utilize this data-driven method to quantitatively establish HGE models of source rocks with different kerogen types based on more considerable Rock-Eval/TOC/VRo datasets. This will help to strengthen research on the differential effects of kerogen types on the HGE characteristics of source rocks and greatly improve the accuracy of resource evaluation.

6. Conclusions

In this study, a data-driven approach was proposed to quantitatively establish an optimized hydrocarbon generation potential model of low-mature to mature source rocks based on abundant Rock-Eval/TOC/VRo datasets, enabling quick and effective source rock evaluation.

This method was applied to the Es4 member of the Niuxintuo area, where thick source rocks (average > 250 m) with high TOC content and low maturity (VRo = 0.26%–0.63%) have developed. Hydrocarbon generation simulation experiments were performed on low-maturity source rocks with different kerogen types to supplement the geochemical characteristics of the source rocks in the mature to high-mature stage. Through numerical analysis of the geochemical datasets, the optimal regression relationships between the GPI, HI, and Ro were fitted. This optimized model determined that the GPIo of the Es4 source rocks is 600 mg HC/g TOC. The HGT and HET are 0.36%VRo and 0.46%VRo, respectively. The hydrocarbon generation intensities of the Es4 member are widely distributed throughout the study area, while the hydrocarbon expulsion intensities are limited to the central part of the Niuxintuo area. The Es4n sub-member has the most considerable conventional and unconventional tight oil and shale oil resources, which are 3.20×10^7 t, 7.70×10^7 t, and 5.93×10^8 t, respectively. The evaluation results of hydrocarbon resources indicate that exploration should focus on tight oil and shale oil in the Niuxintuo area.

This data-driven approach quantifies the HGE capacity of source rocks from the perspective of numerical analysis, reduces the influences of source rock heterogeneity and human subjectivity, and takes into account the loss of TOC. Nevertheless, considerable amounts of geochemical data on source rocks are still needed to further improve the reliability of the model. We will continue to investigate the source rock characteristics of the study area by collecting additional samples and continuously optimizing the HGE model of source rocks. In addition, it is suggested that more detailed research should focus on the differential effects of kerogen types on the HGE characteristics of source rocks based on this data-driven approach.

Author Contributions: Conceptualization, S.H. and X.P.; methodology, S.H., C.L. and K.S.; software, C.L. and S.M.; formal analysis, C.L., K.S., M.L. and J.C.; investigation, X.P. and T.H.; resources, X.Z., W.Y. and J.C.; data curation, X.Z. and S.M.; writing—original draft preparation, S.H.; writing—review and editing, S.H., H.P. and T.H.; visualization, M.L.; supervision, X.P., H.P. and J.C.; project administration, W.Y.; funding acquisition, X.P. All authors have read and agreed to the published version of the manuscript.

Funding: This research was supported by the National Basic Research Program of China (grant number 2011CB201100), the Cooperation Program of PetroChina Liaohe Oilfield Company (grant number HX20180604), and the AAPG Foundation Grants-in-Aid Program (grant number 22269437).

Data Availability Statement: The data that support the findings of this study are available from the corresponding author upon reasonable request.

Acknowledgments: This study benefitted greatly from the data support provided by the PetroChina Liaohe Oilfield Company. We also thank Dingye Zheng and the anonymous reviewers for their professional suggestions.

Conflicts of Interest: The authors declare no competing financial interests.

References

1. Jia, C.Z. Breakthrough and significance of unconventional oil and gas to classical petroleum geological theory. *Pet. Explor. Dev.* **2017**, *44*, 1–10. [CrossRef]
2. EIA. *Technically Recoverable Shale Oil and Shale Gas Resources: An Assessme 137 Shale Formation in 41 Countries Outside the United States*; EIA: Washington, DC, USA, 2013.
3. Labus, K.; Tarkowski, R.; Wdowin, M. Modeling gas–rock–water interactions in carbon dioxide storage capacity assessment: A case study of Jurassic sandstones in Poland. *Int. J. Environ. Sci. Technol.* **2015**, *12*, 2493–2502. [CrossRef]
4. Tarkowski, R.; Wdowin, M.; Manecki, M. Petrophysical examination of CO2-brine-rock interactions—Results of the first stage of long-term experiments in the potential Zaosie Anticline reservoir (central Poland) for CO_2 storage. *Environ. Monit. Assess.* **2015**, *187*, 4251. [CrossRef] [PubMed]
5. Jin, Z.J.; Zhang, J.C. Fundamental principles for petroleum resources assessments. *Acta Pet. Sin.* **2002**, *23*, 19–23.
6. Schmoker, J.W. Resource-assessment perspectives for unconventional gas systems. *AAPG Bull.* **2002**, *86*, 1993–1999.
7. Haskett, W.J.; Brown, P.J. Evaluation of unconventional resource plays. In Proceedings of the SPE Annual Technical Conference and Exhibition, Dallas, TX, USA, 9–12 October 2005.
8. Arab Amiri, M.; Karimi, M.; Abbas, A.S. Hydrocarbon resources potential mapping using evidential belief functions and frequency ratio approaches, southeastern Saskatchewan, Canada. *Can. J. Earth Sci.* **2015**, *52*, 182–195. [CrossRef]
9. Hu, T.; Pang, X.Q.; Jiang, F.J.; Wang, Q.F.; Liu, X.H.; Wang, Z.; Jiang, S.; Wu, G.Y.; Li, C.J.; Xu, T.W.; et al. Movable oil content evaluation of lacustrine organic-rich shales: Methods and a novel quantitative evaluation model. *Earth Sci. Rev.* **2021**, *214*, 103545. [CrossRef]
10. Tissot, B.P.; Welte, D.H. *Petroleum Formation and Occurrence*; Springer: New York, NY, USA, 1984.
11. Jarvie, D.M.; Hill, R.J.; Ruble, T.E.; Pollastro, R.M. Unconventional shale-gas systems: The Mississippian Barnett Shale of north-central Texas as one model for thermogenic shale-gas assessment. *AAPG Bull.* **2007**, *91*, 475–499. [CrossRef]
12. Pang, X.Q.; Li, M.W.; Li, S.M.; Jin, Z.J. Geochemistry of petroleum systems in the Niuzhuang South Slope of Bohai Bay Basin: Part 3. Estimating hydrocarbon expulsion from the Shahejie formation. *Org. Geochem.* **2005**, *36*, 497–510. [CrossRef]
13. Peng, J.W.; Pang, X.Q.; Shi, H.S.; Peng, H.J.; Xiao, S.; Yu, Q.H.; Wu, L.Y. Hydrocarbon generation and expulsion characteristics of Eocene source rocks in the Huilu area, northern Pearl River Mouth basin, South China Sea: Implications for tight oil potential. *Mar. Pet. Geol.* **2016**, *72*, 463–487. [CrossRef]
14. Zheng, D.Y.; Pang, X.Q.; Ma, X.H.; Li, C.R.; Zheng, T.Y.; Zhou, L.M. Hydrocarbon generation and expulsion characteristics of the source rocks in the third member of the Upper Triassic Xujiahe Formation and its effect on conventional and unconventional hydrocarbon resource potential in the Sichuan Basin. *Mar. Pet. Geol.* **2019**, *109*, 175–192. [CrossRef]
15. Wang, E.Z.; Liu, G.Y.; Pang, X.Q.; Li, C.R.; Zhao, Z.F.; Feng, Y.; Wu, Z.Y. An improved hydrocarbon generation potential method for quantifying hydrocarbon generation and expulsion characteristics with application example of Paleogene Shahejie Formation, Nanpu Sag, Bohai Bay Basin. *Mar. Pet. Geol.* **2020**, *112*, 104106. [CrossRef]
16. Li, C.R.; Pang, X.Q.; Huo, Z.P.; Wang, E.Z.; Xue, N. A revised method for reconstructing the hydrocarbon generation and expulsion history and evaluating the hydrocarbon resource potential: Example from the first member of the Qingshankou Formation in the Northern Songliao Basin, Northeast China. *Mar. Pet. Geol.* **2020**, *121*, 104577. [CrossRef]
17. Li, M.; Pang, X.Q.; Luo, B.; Wang, W.; Cao, L.Y.; Hu, T.; Hui, S.S.; Li, C.R. Application of hydrocarbon generation potential method to deep shale gas resource evalution: A case study of high-quality source rocks of the Wufeng-Longmaxi formation in the Sichuan Basin. *J. China Uni. Min. Technol.* **2021**, *50*, 1096–1107.
18. Chen, J.Q.; Pang, X.Q.; Pang, H.; Chen, Z.H.; Jiang, C.Q. Hydrocarbon evaporative loss evaluation of lacustrine shale oil based on mass balance method: Permian Lucaogou Formation in Jimusaer Depression, Junggar Basin. *Mar. Pet. Geol.* **2018**, *91*, 422–431. [CrossRef]
19. Justwan, H.; Dahl, B. Quantitative hydrocarbon potential mapping and organofacies study in the Greater Balder area, Norwegian North Sea. In *Petroleum Geology Conference Series*; Dore, A.G., Vinino, A., Eds.; Geological Society: London, UK, 2005; pp. 1317–1329.
20. Li, X.G. Accumulation conditions and key exploration & development technologies of heavy oil in Huanxiling oilfield in Liaohe depression, Bohai Bay Basin. *Pet. Res.* **2020**, *5*, 18–38.
21. Hao, F.; Zhou, X.; Zhu, Y.; Zou, H.; Yang, Y. Charging of oil fields surrounding the Shaleitian uplift from multiple source rock intervals and generative kitchens, Bohai Bay basin, China. *Mar. Pet. Geol.* **2010**, *27*, 1910–1926. [CrossRef]
22. Allen, M.B.; Macdonald, D.I.M.; Xun, Z.; Vincent, S.J.; Brouet-Menzies, C. Early Cenozoic two-phase extension and late Cenozoic thermal subsidence and inversion of the Bohai Basin, northern China. *Mar. Pet. Geol.* **1997**, *14*, 951–972. [CrossRef]

23. Hu, L.G.; Fuhrmann, A.; Poelchau, H.S.; Horsfield, B.; Zhang, Z.W.; Wu, T.S.; Chen, Y.; Li, J. Numerical simulation of petroleum generation and migration in the Qingshui sag, western depression of the Liaohe basin, northeast China. *AAPG Bull.* **2005**, *89*, 1629–1649. [CrossRef]
24. Wei, W.; Zhu, X.M.; Meng, Y.L.; Xiao, L.H.; Xue, M.G.; Wang, J.Y. Porosity model and its application in tight gas sandstone reservoir in the southern part of West Depression, Liaohe Basin, China. *J. Pet. Sci. Eng.* **2016**, *141*, 24–37. [CrossRef]
25. Hao, F.; Zhou, X.; Zhu, Y.; Yang, Y. Lacustrine source rock deposition in response to co-evolution of environments and organisms controlled by tectonic subsidence and climate, Bohai Bay Basin, China. *Org. Geochem.* **2011**, *42*, 323–339. [CrossRef]
26. Meng, Y.; Zhang, L.; Qu, G.; Zhang, F.; Meng, F.; Li, C.; Jiao, J.; Shi, L. Diagenetic characteristics under abnormally low pressure: A case from the Paleogene of southern Western Sag, Liaohe Depression, Bohai Bay Basin. *Pet. Explor. Dev.* **2016**, *43*, 731–736. [CrossRef]
27. Pang, S.Y.; Cao, Y.C.; Liang, C. Lithofacies characteristics and sedimentary environment of Es4U and Es3L: A case study of Well FY1 in Dongying sag, Bohai Bay Basin. *Oil Gas Geol.* **2019**, *40*, 799–809. (In Chinese)
28. Peters, K.E. Guidelines for evaluating petroleum source rock using programmed pyrolysis. *AAPG Bull.* **1986**, *70*, 318–329.
29. Riediger, C.; Carrelliand, G.G.; Zonneveld, J.P. Hydrocarbon source rock characterization and thermal maturity of the Upper Triassic Baldonnel and Pardonet formations, northeastern British Columbia, Canada. Bulletin of Canadian. *Petrol. Geol.* **2004**, *52*, 277–301.
30. *SY/T 5124—2012*; National Energy Administration. Method of Determining Microscopically the Reflectance of Vitrinite in Sedimentary. Petroleum Industry Press: Beijing, China,, 2012.
31. *SY/T 6414—2014*; National Energy Administration. Maceral Identification and Statistical Methods on Polished Surfaces of Whole Rocks. Petroleum Industry Press: Beijing, China, 2014.
32. Chen, J.Q.; Zhang, X.G.; Chen, Z.H.; Pang, X.Q.; Yang, H.J.; Zhao, Z.F.; Pang, B.; Ma, K.Y. Hydrocarbon expulsion evaluation based on pyrolysis Rock-Eval data: Implications for Ordovician carbonates exploration in the Tabei Uplift, Tarim. *J. Pet. Sci. Eng.* **2021**, *196*, 107614. [CrossRef]
33. Cooles, G.P.; Mackenzie, A.S.; Quigley, T.M. Calculation of petroleum masses generated and expelled from source rocks. *Org. Geochem.* **1986**, *10*, 235–245. [CrossRef]
34. Bordenave, M.L.; Espitalie, J.; Leplat, J.L.; Vandenbroucke, M. Screening techniques for source rock evaluation. In *Applied Petroleum Geochemistry*; Bordenave, M.L., Ed.; Editions Technips: Paris, France, 1993; pp. 217–278.
35. Chen, Z.H.; Jiang, C.Q. A data driven model for studying kerogen kinetics with application examples from Canadian sedimentary basins. *Mar. Pet. Geol.* **2015**, *67*, 795–803. [CrossRef]
36. Chen, Z.H.; Jiang, C.Q. A revised method for organic porosity estimation in shale reservoirs using Rock—Eval data: Example from Duvernay Formation in the Western Canada Sedimentary Basin. *AAPG Bull.* **2016**, *100*, 405–422. [CrossRef]
37. White, I.C. The geology of natural gas. *Science* **1885**, *6*, 42–44. [CrossRef]
38. Masters, J.A. Deep basin gas trap, Western Canada. *AAPG Bull.* **1979**, *63*, 152–181.
39. Pang, X.Q.; Jia, C.Z.; Wang, W.Y.; Chen, Z.X.; Li, M.W.; Jiang, F.J.; Hu, T.; Wang, K.; Wang, Y.X. Buoyance-driven hydrocarbon accumulation depth and its implication for unconventional resource prediction. *Geosci. Front.* **2021**, *12*, 101133. [CrossRef]
40. Huang, S.P.; Feng, Z.Q.; Gu, T.; Gong, D.Y.; Peng, W.L.; Yuan, M. Multiple origins of the Paleogene natural gases and effects of secondary alteration in Liaohe Basin, northeast China: Insights from the molecular and stable isotopic compositions. *Int. J. Coal Geol.* **2017**, *172*, 134–148. [CrossRef]
41. Peng, W.L.; Hu, G.Y.; Feng, Z.Q.; Liu, D.; Wang, Y.W.; Lv, Y.; Zhao, R.M. Origin of Paleogene natural gases and discussion of abnormal carbon isotopic composition of heavy alkanes in the Liaohe Basin, NE China. *Mar. Pet. Geol.* **2018**, *92*, 670–684. [CrossRef]
42. Mackenzie, A.S.; Maxwell, J.R.; Coleman, M.L.; Deegan, C.E. Biological marker and isotope studies of North Sea crude oils and sediments. In Proceedings of the Eleventh World Petroleum Congress, London, UK, 28 August–2 September 1983; John Wiley and Sons: New York, NY, USA, 1984.
43. Chen, J.Y.; Bi, Y.P.; Zhang, J.G.; Li, S.F. Oil-source correlation in the Fulin basin, Shengli petroleum province, East China. *Org. Geochem.* **1996**, *24*, 931–940. [CrossRef]
44. Huo, Z.; Tang, X.; Meng, Q.; Zhang, J.; Li, C.; Yu, X.; Yang, X. Geochemical characteristics and hydrocarbon expulsion of lacustrine marlstones in the Shulu sag, Bohai bay basin, eastern China: Assessment of tight oil resources. *Nat. Resour. Res.* **2020**, *29*, 2647–2669. [CrossRef]
45. Bazhenova, O.K.; Arefiev, O.A.; Durand, B.; Behar, F. Immature oils as the products of early catagenetic transformation of bacterial-algal organic matter. *Org. Geochem.* **1990**, *16*, 307–311. [CrossRef]
46. Wang, F.Y.; Hao, S.S.; He, P.; Fu, J.M. Lacustrine algae in Biyang sag as high wax oleaginous parent material. *Chin. Sci. Bull.* **1997**, *42*, 1193–1197.
47. Liu, W.H.; Huang, D.F.; Xiong, C.W.; Xu, Y.C. The development of hydrocarbon generation theory and the distribution and research status of immature and low-mature oil/gas abroad. *Nat. Gas Geosci.* **1999**, *10*, 1–22.
48. Zhao, X.Z.; Ma, A.L.; Xiong, B.; Zhong, N.N.; Wang, T.G. Organic petrological characteristics of immature source rocks. *Geol. Geochem.* **2002**, *30*, 20–25.
49. Guo, B.; Ma, S.M.; Li, M.; Wang, X.H.; Xi, J.; Wang, C.J.; Jiang, R.Y. Hydrocarbon generation potential and features of lamellar algae in Shanxi Hunyuan. *Coal. Coal Sci. Technol.* **2011**, *39*, 106–109.

50. Adeyilola, A.; Zakharova, N.; Liu, K.; Gentzis, T.; Carvajal-Ortiz, H.; Ocubalidet, S.; Harrison, W.B. Hydrocarbon potential and Organofacies of the Devonian Antrim Shale, Michigan Basin. *Int. J. Coal Geol.* **2022**, *249*, 103905. [CrossRef]
51. Pang, X.Q.; Liu, K.Y.; Ma, Z.Z.; Jiang, Z.X.; Xiang, C.F.; Huo, Z.P.; Pang, H.; Chen, J.Q. Dynamic field division of hydrocarbon migration, accumulation and hydrocarbon enrichment rules in sedimentary basins. *Acta Geol. Sin.* **2012**, *86*, 1559–1592.
52. Jia, C.Z.; Zou, C.N.; Li, J.Z.; Li, D.H.; Zheng, M. Assessment criteria, main types, basic features and resource prospects of the tight oil in China. *Acta Pet. Sin.* **2012**, *33*, 343–350. (In Chinese)
53. Guo, Y.; Pang, X.; Li, Z.; Guo, F.; Song, L. The critical buoyancy threshold for tight sandstone gas entrapment: Physical simulation, interpretation, and implications to the Upper Paleozoic Ordos Basin. *J. Pet. Sci. Eng.* **2017**, *149*, 88–97. [CrossRef]